

Measurement report: Nitrogen isotopes ($\delta^{15}\text{N}$) and first quantification of oxygen isotope anomalies ($\Delta^{17}\text{O}$, $\delta^{18}\text{O}$) in atmospheric nitrogen dioxide

Sarah Albertin^{1,2}, Joël Savarino², Slimane Bekki¹, Albane Barbero², and Nicolas Caillon²

5 ¹LATMOS/IPSL, Sorbonne Université, UVSQ, CNRS, 75005 Paris, France

²IGE, Univ. Grenoble Alpes, CNRS, IRD, Grenoble INP, 38000 Grenoble, France

Correspondence to: Sarah Albertin (sarah.albertin@latmos.ipsl.fr)

Abstract. The isotopic composition of nitrogen and oxygen in nitrogen dioxide (NO_2) potentially carries a wealth of information about the dynamics of the nitrogen oxides ($\text{NO}_x = \text{nitric oxide (NO)} + \text{NO}_2$) chemistry in the atmosphere.

10 While nitrogen isotopes of NO_2 are subtle indicators of NO_x emissions and chemistry, oxygen isotopes are believed to reflect only the $\text{O}_3/\text{NO}_x/\text{VOC}$ chemical regime in different atmospheric environments. In order to access this potential tracer of the tropospheric chemistry, we have developed an efficient active method to trap atmospheric NO_2 on denuder tubes and measured, for the first time, its multi-isotopic composition ($\delta^{15}\text{N}$, $\delta^{18}\text{O}$, and $\Delta^{17}\text{O}$). The $\Delta^{17}\text{O}$ values of NO_2 trapped at our site in Grenoble, France, show a large diurnal cycle peaking in late morning at $(39.2 \pm 0.3) \text{ ‰}$ and decreasing at night until $(20.5 \pm 0.3) \text{ ‰}$. On 15 top of this diurnal cycle, $\Delta^{17}\text{O}$ also exhibits substantial daytime variability (from 29.7 to 39.2 ‰), certainly driven by changes in the O_3 to peroxy radicals (RO_2) ratio. The nighttime decay of $\Delta^{17}\text{O}(\text{NO}_2)$ appears to be driven by NO_2 slow removal, mostly from conversion into N_2O_5 , and its formation from the reaction between O_3 and freshly emitted NO. As expected from a nighttime $\Delta^{17}\text{O}(\text{NO}_2)$ expression, our $\Delta^{17}\text{O}(\text{NO}_2)$ measured towards the end of the night is quantitatively consistent with typical values of $\Delta^{17}\text{O}(\text{O}_3)$. Daytime N isotope fractionation is estimated using a general expression linking it to $\Delta^{17}\text{O}(\text{NO}_2)$. An 20 expression is also derived for the nighttime N isotope fractionation. In contrast to $\Delta^{17}\text{O}(\text{NO}_2)$, $\delta^{15}\text{N}(\text{NO}_2)$ measurements exhibit little diurnal variability (-11.8 to -4.9 ‰) with negligible isotope fractionations between NO and NO_2 , mainly due to high NO_2/NO_x ratios, excepted during the morning rush hours. The main NO_x emissions sources are estimated using a Bayesian 25 isotope mixing model, indicating the predominance of traffic emissions in this area. These preliminary results are very promising for using the combination of $\Delta^{17}\text{O}$ and $\delta^{15}\text{N}$ of NO_2 as a probe of the NO_x sources and fate and for interpreting nitrate isotopic composition records.

1 Introduction

Nitrogen oxides ($\text{NO}_x = \text{NO}_2 + \text{NO}$) are at the heart of tropospheric chemistry, as they are involved in key reaction chains governing the production and destruction of compounds of fundamental interest for health, ecosystems and climate issues (Brown, 2006; Finlayson-Pitts and Pitts, 2000; Jacob, 1999). For example, NO_2 photolysis followed by reaction of NO with 30 peroxy radicals ($\text{RO}_2 = \text{HO}_2 + \text{RO}_2$) is the only significant source of ozone (O_3) in the troposphere where it serves as a severe air pollutant and a greenhouse gas. Tropospheric O_3 also plays a major role in the production processes of radicals which are

responsible for the oxidation and removal of compounds emitted into the atmosphere (Crutzen, 1996). This “cleaning” ability is referred to as the atmospheric oxidative capacity (AOC; Prinn, 2003). Additionally, NO_x species are at the core of the reactive nitrogen cycle as precursors of atmospheric nitrate (particulate NO_3^- + gaseous HNO_3) which contributes to soil acidification and eutrophication (Galloway et al., 2004), and aerosol radiative forcing (Liao and Seinfeld, 2005). In order to better understand the reactive nitrogen (which includes NO_x and HNO_3) chemistry, the related AOC, and the contributions of precursor emissions to nitrate deposition, it is necessary to better constrain NO_x emission sources and individual oxidation processes.

Stable isotope analysis is a powerful tool for tracing emission sources, individual chemical mechanisms and budgets of atmospheric trace gases (Kaye, 1987). Because physico-chemical and biological processes favour lighter or heavier isotopologues, the isotopic composition of a chemical species will often vary according to its formation pathway. This phenomenon of isotopic fractionation can thus be used to trace different processes involved in the formation of the chemical species being analyzed. Isotopic enrichment (δ) of an element X is expressed in ‰ and defined as: $\delta^{\text{X}} = ({}^{\text{n}}R_{\text{spl}} / {}^{\text{n}}R_{\text{ref}} - 1)$ with ${}^{\text{n}}R$ the elemental isotope abundance ratio of the heavy isotope over the light isotope (e.g. for oxygen isotopes ${}^{18}R = {}^{18}\text{O} / {}^{16}\text{O}$) with ${}^{18}R = x({}^{18}\text{O}) / x({}^{16}\text{O})$ or ${}^{17}R = x({}^{17}\text{O}) / x({}^{16}\text{O}) \equiv {}^{17}R = x({}^{17}\text{O}) / x({}^{16}\text{O})$, with x the isotopic abundance) in a sample (${}^{\text{n}}R_{\text{spl}}$) and in a reference (${}^{\text{n}}R_{\text{ref}}$). The Vienna Standard Mean Ocean Water (VSMOW; Li et al., 1988) and atmospheric nitrogen (N_2 ; Mariotti, 1984) are the international references for oxygen and nitrogen ratios, respectively. Most natural isotopic fractionations are mass dependent fractionations (MDF; Urey, 1947), as it is notably the case for terrestrial oxygenated species in which the triple oxygen composition follows $\delta^{17}\text{O} \approx 0.52 \times \delta^{18}\text{O}$ (Thiemens, 1999). Yet, laboratory experiments (Thiemens and Heidenreich, 1983) and atmospheric observations (Johnston and Thiemens, 1997; Krankowsky et al., 1995; Vicars and Savarino, 2014) have showed that the isotopic composition of ozone formed in the atmosphere does not follow this canonical MDF relationship and reflects mass independent fractionation (MIF) processes. The important deviation from the MDF oxygen relationship is called the oxygen-17 anomaly ($\Delta^{17}\text{O}$) and is defined here in its approximate linearized form as $\Delta^{17}\text{O} = \delta^{17}\text{O} - 0.52 \times \delta^{18}\text{O}$. Our choice of this linear definition is mainly motivated by its convenience for mass balance calculations and its validity for our large $\Delta^{17}\text{O}$ values and variability. Overall, biases related to our choice of the linear definition are marginal in our conditions (Assonov and Brenninkmeijer, 2005). It follows that $\Delta^{17}\text{O}$ inherited from ozone can be considered as conserved during MDF processes.

The multi-isotopic composition of NO_x is therefore a very valuable tracer of its emissions and chemistry in the atmosphere. However, so far, $\Delta^{17}\text{O}$ of atmospheric NO_2 ($\Delta^{17}\text{O}(\text{NO}_2)$) has been investigated only using laboratory (Michalski et al., 2014) and modelling (Alexander et al., 2020, 2009; Lyons, 2001; Morin et al., 2011) approaches with theoretical frameworks, and these results need to be tested against atmospheric observations. Walters et al. (2018) have presented a method of sampling and analysing nitrogen and oxygen stable isotopes of NO_2 collected separately at daytime and nighttime in an urban area but they did not report on $\Delta^{17}\text{O}$. Dahal and Hastings (2016) have attempted to measure $\Delta^{17}\text{O}$ of NO_2 collected on passive samplers, but the isotopic signal was partly degraded during the sampling and the analytical procedure. Building on their work, we

65 present here an efficient method to collect atmospheric NO₂ for isotopic analysis and present the first measurements of triple oxygen isotopes and double nitrogen isotopes of atmospheric NO₂. Combined with mass-balance equations, oxygen isotopes are used to investigate the links between the variability of the oxygen isotope anomaly of NO₂ and its formation pathways. We also revisit the Morin et al. (2011) NO_x isotopic theoretical framework and extend it to urban environments. After estimating the nitrogen isotopic fractionation between NO and NO₂, we infer from $\delta^{15}\text{N}$ of NO₂ ($\delta^{15}\text{N}(\text{NO}_2)$) the major emission sources
70 of NO_x influencing our sampling site using an isotopic mixing model (Parnell et al., 2010).

2 Materials and Methods

2.1 Sampling method

NO₂ was sampled on an active (pumped) collection system using denuder tubes. This method is more efficient to collect NO₂ than passive methods (Røyset, 1998), allowing for shorter collection times with a breakthrough of the absorption capacity
75 below 1 % (Buttini et al., 1987; Williams and Grosjean, 1990). The sampled air was pumped through a ChemComb® 3500 speciation cartridge (Thermo Scientific®, USA). Initially used for the speciation of gases and aerosols, these advanced sampling platforms consist of a PM_{2.5} impactor inlet connected to a stainless-steel cylinder that contains two glass honeycomb denuders connected in series for gas collection, and a Teflon stage filter pack for aerosols. To collect NO₂, glass tubes were coated with an alkaline guaiacol solution. In basic medium, guaiacol (IUPAC name: 2-Methoxyphenol) is known to react with NO₂ to form
80 stable NO₂⁻ ions (Nash, 1970) preserving the original NO₂ isotopic signal due to the basic nature of the medium (pH = 14 after 10 ml extraction). Because NO or peroxyacetyl nitrate (PAN) are not collected by guaiacol, this methodology avoids potential interferences from these compounds in later analyses (Buttini et al., 1987). Although nitrous acid (HONO) can bind as NO₂⁻, it is unlikely to adversely impact the results as its mixing ratio (i.e. mole fraction) is much lower than NO₂ (by a factor of 10 to 20) even in very polluted cities (e.g., Harris et al., 1982; Michoud et al., 2014; Huang et al., 2017).
85 To evaluate the sampling system performance, a series of experiments were run with artificial gaseous NO₂. Using a commercial gas standard generator (KinTek FlexStream®) feed with zero-air, diluted NO₂ (Metronics Dynacal®) was sent through a ChemComb cartridge while NO_x mixing ratio was measured up- and down-stream of the cartridge. From 1 to 30 nmol mol⁻¹ of NO₂ (representative of rural to urban atmospheric conditions), mixing ratios coming out of the cartridge were never above the noise level of the NO_x monitor (2.5 nmol mol⁻¹). To estimate the denuders trapping efficiency, we passed
90 different mixing ratios of gaseous NO₂ through the collection apparatus and measured the amount of NO₂⁻ collected on the two denuders both connected in series. The denuder efficiency E was then calculated according to the following equation (Buttini et al., 1987):

$$E = (1 - \frac{b}{a}) \times 100 \% \quad (1)$$

with a and b representing the amount of NO₂⁻ collected on the first and the second denuder, respectively. From 0.3 to 1.3 μmol
95 of generated NO₂ (see Fig. 1), the mean E value was about $(97 \pm 3) \%$. The amount of NO₂⁻ measured on second denuders was

reproducible and equivalent to blanks, representing on average 3 % of the quantity measured on the first denuders. In light of these results, denuders in second position were not subjected to isotopic analysis and allowed trapping efficiency control.

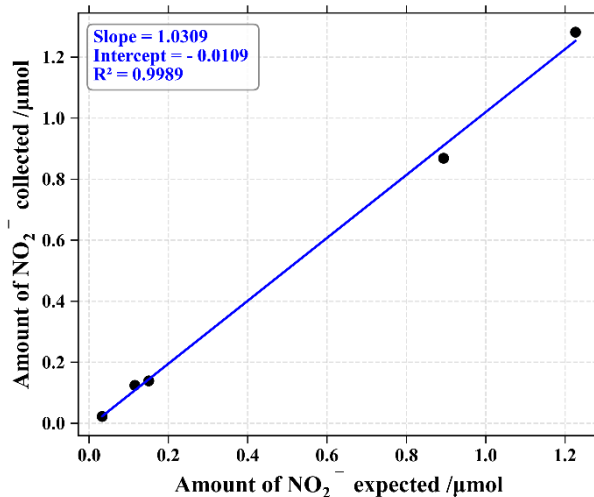


Figure 1. Correlation plot of NO_2 collected on the first denuder tube of the sampling cartridge vs. NO_2 produced by the gas standard generator.

110 2.2 Isotopic analysis

Simultaneous isotopic analyses of $\delta^{15}\text{N}$, $\delta^{18}\text{O}$, and $\delta^{17}\text{O}$ were performed using a Finnigan[®]-MAT253 isotope ratio mass spectrometer (IRMS) following techniques described by Casciotti et al. (2002) and Kaiser et al. (2007). The azide method (McIlvin and Altabet, 2005) was used with ≈ 100 nmol of nitrites converted to N_2O using a 50:50 by volume mixture of 2 M sodium azide and 100 % acetic acid. This chemical method has the advantage over the bacterial method to be free of nitrate interferences since HNO_3 is certainly trapped with NO_2 in the basic solution coating of the denuder tube. The principle of identical treatment (Brand, 1996) was strictly respected where the standards and samples possessed the same nitrite amount, water isotopes, total volume and matrix. Three international KNO_2 salt standards, RSIL-N7373, RSIL-N10219, and RSIL-N23 with respective $\delta^{15}\text{N}/\delta^{18}\text{O}$ values of $-79.6/4.2\text{ ‰}$, $2.8/88.5\text{ ‰}$, and $3.7/11.4\text{ ‰}$ were used for normalisation of δ -scale. Scale contraction factors were obtained with the linear regression between measured and known values of $\delta^{15}\text{N}$ and $\delta^{18}\text{O}$. Although the three standards cover a wide range of isotopic composition in $\delta^{15}\text{N}$ and $\delta^{18}\text{O}$, they do not have an isotopic anomaly in $\delta^{17}\text{O}$. For $\delta^{17}\text{O}$ -scale, MDF fractionation slope (0.52) is assumed for two of these laboratory-prepared nitrite standards (see Appendix A for more details). Accuracy of this analytical method on $\delta^{17}\text{O}$, $\delta^{18}\text{O}$ and $\delta^{15}\text{N}$ measurements was estimated as the standard deviation (σ) of the residuals between our measurements of the RSIL standards and their expected values. Additionally, isotopic integrity from denuders extraction to the analysis by IRMS has been investigated and showed no degradation over several weeks (see Appendix B) confirming that this method is suitable for isotopic analysis of NO_2 , as first demonstrated by

Walters et al. (2018). The uncertainties applied to our measurements of $\delta^{15}\text{N}$, $\delta^{17}\text{O}$ and $\delta^{18}\text{O}$ are reported as the propagation error of the measurement uncertainty and the uncertainty resulting from sample storage. Uncertainty on $\Delta^{17}\text{O}$ is derived from the propagation error of the overall uncertainty on $\delta^{17}\text{O}$ and $\delta^{18}\text{O}$. In our study, average uncertainties on $\delta^{15}\text{N}$, $\delta^{17}\text{O}$, $\delta^{18}\text{O}$, and $\Delta^{17}\text{O}$ are estimated to be ± 0.1 , ± 0.8 , ± 1.8 and $\pm 0.3\text{‰}$, respectively (1σ uncertainties).

130 2.3 Study site and atmospheric NO_2 collection

Atmospheric NO_2 was collected at the Université Grenoble Alpes campus site. Located to the eastern Grenoble urban area (690 000 inhabitants), the campus stands between a major transportation route and the Isère river. The city is located at the confluence of three valleys surrounded by mountain chains that influence the atmospheric dynamics and the local air quality. During winter, persistent temperature inversions combined with intense domestic heating can lead to severe PM_{10} pollution 135 events (Largeron and Staquet, 2016) with daily-average mixing ratio above World Health Organisation thresholds. In summer, emissions are mainly controlled by road traffic that can result in heightened ozone mixing ratios, especially during stagnant conditions.

Samplings were conducted on a platform five meters above the ground surface. Ambient air was drawn through the cartridge with a Millipore vacuum pump at a flow rate of 10 L min^{-1} (room temperature and one atmospheric pressure) adjusted using a 140 Cole-Palmer[®] flowmeter (accuracy $\pm 3\text{ %}$). In order to capture the daily variability in NO_2 isotopic composition, samples were collected during 24 hours with 3 h sampling intervals during the day, and 5 h sampling from midnight to 05:00. Ambient NO and NO_2 mixing ratios were measured with a 2B Technologies[®] NO monitor model 410 paired with a NO_2 converter model 401.

Honeycomb denuders were cleaned and coated the day before sampling. After being generously rinsed (5 minutes under a 145 stream of deionised water), the denuders were placed in a vacuum chamber (Thermo Scientific[®] Refrigerated VaporTrap paired with a SpeedVac Concentrator) and dried at 40°C during 1 hour. Then, denuders internal walls were individually coated with 10 ml of a 95:5 by volume mixture of 2.5 M KOH (in methanol) and ultrapure guaiacol prepared daily. Denuders were then drawn off, dried in the vacuum chamber at 40°C during 30 minutes to minimize blanks, hermetically sealed and stored at ambient temperature in the dark until usage. The different components of the cartridge (impactor, filters, denuders) were 150 cleaned, dried and fitted together just before use. At the end of the sampling period both denuders were removed from the ChemComb cartridge and rinsed with 10 ml of deionised water in order to leach trapped NO_2 out. 1 ml of the eluent was rapidly used to determine the nitrite amount using the Griess-Saltzman reaction and UV-vis spectrometry at 544 nm. Recovered eluent (≈ 7 ml by denuder) was poured in a labelled 15 ml Corning[®] and stored in a freezer until isotopic analysis the following days.

3.1 NO_x and O₃ atmospheric observations

Figure 2 shows the time evolution of the hourly NO₂, NO and, O₃ mixing ratios measured during the period covering two nights and one day (from 14 May 2019 21:00 to 16 May 2019 05:00). Note that most of our NO measurements are found to be within the reported detection limit of the instrument except in the morning (see Table 1) and therefore, have to be treated with lot of caution. NO₂ mixing ratios during the sampling period ($(6.1 \pm 4.2) \text{ nmol mol}^{-1}$; mean \pm one standard deviation) are in good agreement with the range of values measured at the local air quality site located a kilometre south of the sampling site (<https://www.atmo-auvergnerhonealpes.fr/>).

During both nights, most of the NO_x are in the form of NO₂. After sunrise, there is a rapid interconversion between NO and NO₂, driven by NO₂ photolysis and reactions of NO with O₃ and peroxy radicals (Jacob, 1999). NO₂ levels are maximum on 160 15 May between 04:00 and 10:00 with a sharp peak of 21 nmol mol⁻¹ at 08:00. After the morning rise, NO₂ decreases to reach a background mixing ratio of about $(3.0 \pm 0.5) \text{ nmol mol}^{-1}$. This diurnal variation is common in urban/suburban sites characterised by a morning peak caused by important NO_x emissions, mainly from road traffic (Mayer, 1999). As morning progresses, the boundary layer height increases rapidly, favouring fast dilution of NO_x mixing ratios. Moreover, during the day, NO₂ is converted to HNO₃, notably by its reaction with OH radicals. Thus, NO_x mixing ratio remains low during the day 165 likely because of the combination of atmospheric dilution by vertical mixing and efficient chemical conversion by OH and organic radicals (Tie et al., 2007). In dense urban areas, a second NO_x traffic emission peak can occur in late afternoon but it is not observed at our sampling site for that specific day. This surface pollution peak is usually weaker than the morning peak due to an elevated boundary layer and a longer period of evening commuting. After sunset, NO₂ mixing ratio increases gently 170 and reaches a smooth peak with a maximum of 12 nmol mol⁻¹ around 01:00, also recorded at the local air quality site. This NO₂ mixing ratio rise may be due to low NO emissions (converted to NO₂ by reaction with O₃) combined with a decreasing boundary layer height during the night which traps atmospheric species close to the surface (Tie et al., 2007; Villena et al., 175 2011).

Ozone also exhibits a diurnal variation typical of urban areas (Velasco et al., 2008). O₃ peaks around 50 nmol mol⁻¹ at the beginning of both nights to then declines continuously. Indeed, after sunset, O₃ production ceases and its mixing ratio drops 180 due to its dry deposition, reactions with organics, and O₃ titration by NO emitted from evening traffic, and industrial activities in the stable nocturnal boundary layer (Klein et al., 2019). O₃ reaches a minimum (about 15 nmol mol⁻¹) not at the end of the night but during the morning rush hours peak of NO. O_x ($= O_3 + NO_2$) is a more conservative quantity than O₃ because it is less affected by conversion of O₃ into NO₂ through NO titration which is important in urban environments (Kleinman et al., 2002). For instance, between 06:00 and 08:00, O₃ is strongly titrated by freshly emitted NO with its mixing ratio dropping to 185 about 15 nmol mol⁻¹ while O_x reaches a moderate minimum of 34 nmol mol⁻¹. After this morning drop, O₃ recovers rapidly to about 46 nmol mol⁻¹ in the late morning, possibly caused by downward O₃ flux associated with the formation of the day-time thick boundary layer (Jin and Demerjian, 1993; Klein et al., 2019). During the rest of the day, O₃ and O_x keep increasing

gently due to photochemical production and reach a close maximum at the end of the afternoon (Geng et al., 2008). After sunset, the important decline of both O_3 and O_x highlights the physical losses, notably O_3 deposition, and chemical loss of NO_x , typical of urban area.

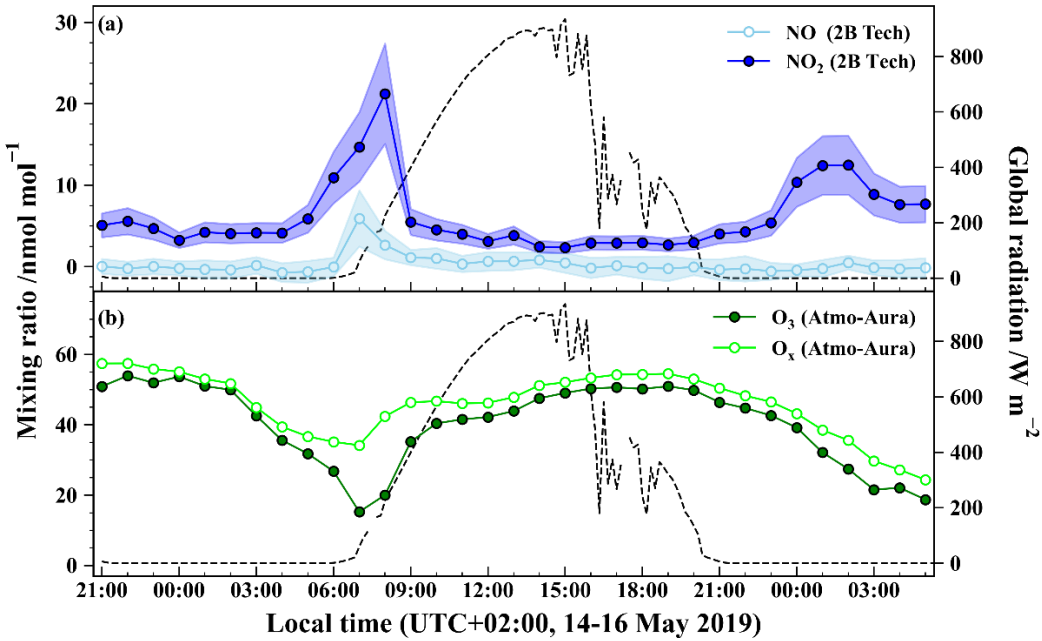


Figure 2. Temporal evolution of (a) NO (open circles) and NO_2 (close circles) at the sampling site (the envelopes represent $\pm 1\sigma$ variations over 1 hour) and of (b) O_3 (close circles) and O_x ($= O_3 + NO_2$; open circles) at the air quality station during the sampling period. Markers represent for (a) the hourly mean derived from 1-min measurements and for (b) the hourly mean provided by the air quality monitoring station. Global solar radiation flux is represented by dashed lines (measured at 200 meters from the sampling site by the IGE weather station with a Skye SP1110 pyranometer).

We present the data for the multi-isotopic composition of seven atmospheric NO_2 samples while two additional samples were rejected as NO_2^- amounts were too low to perform a reliable analysis. Table 1 reports ambient mean mixing ratios of NO, NO_2 and, O_3 for the isotopic sampling intervals and corresponding measured NO_2 isotopic composition ($\delta^{15}N(NO_2)$, $\delta^{18}O(NO_2)$, and $\Delta^{17}O(NO_2)$). Figure 3 depicts the time series of measured $\delta^{15}N$, $\delta^{18}O$, and $\Delta^{17}O$ of atmospheric NO_2 . The temporal evolution of NO_2 oxygen and nitrogen isotopic composition is interpreted in the following section.

Local sampling date & time (start - end)	NO (± 2.5 nmol mol $^{-1}$)	NO ₂ (± 2.5 nmol mol $^{-1}$)	O ₃ ^(*) (± 0.1 ‰)	$\delta^{15}\text{N}(\text{NO}_2)$ (± 1.8 ‰)	$\delta^{18}\text{O}(\text{NO}_2)$ (± 0.3 ‰)	$\Delta^{17}\text{O}(\text{NO}_2)$ (± 0.3 ‰)
14 May 2019 21:00 - 00:00	0.0	5.1	52.3	-11.7	75.6	27.4
15 May 2019 06:00 - 09:00	2.9	15.6	20.7	-4.9	97.6	31.8
15 May 2019 09:00 - 12:00	0.8	4.7	39.1	-10.1	114.5	39.2
15 May 2019 12:00 - 15:00	0.7	3.1	44.6	-11.8	90.9	35.8
15 May 2019 15:00 - 18:00	0.2	2.7	50.0	-11.0	86.9	31.1
15 May 2019 18:00 - 21:00	0.0	2.9	50.3	-11.1	77.1	29.7
16 May 2019 00:00 - 05:00	0.0	9.9	26.9	-11.1	62.2	20.5

Table 1. Summary table of sampling periods (dates, local times), NO, NO₂ and O₃ mean mixing ratios over the collection periods, and calibrated NO₂ isotopic measurements of $\delta^{15}\text{N}$, $\delta^{18}\text{O}$, and $\Delta^{17}\text{O}$. All the sampling periods lasted 3 hours except the last one that lasted 5 hours. Averaged measurement uncertainties are provided just below the species names. ^(*) Data monitored at the local air quality monitoring site of Saint-Martin d'Hères located a kilometre south of the sampling site (<https://www.atmo-auvergnerhonealpes.fr/>).

220

225

230

235

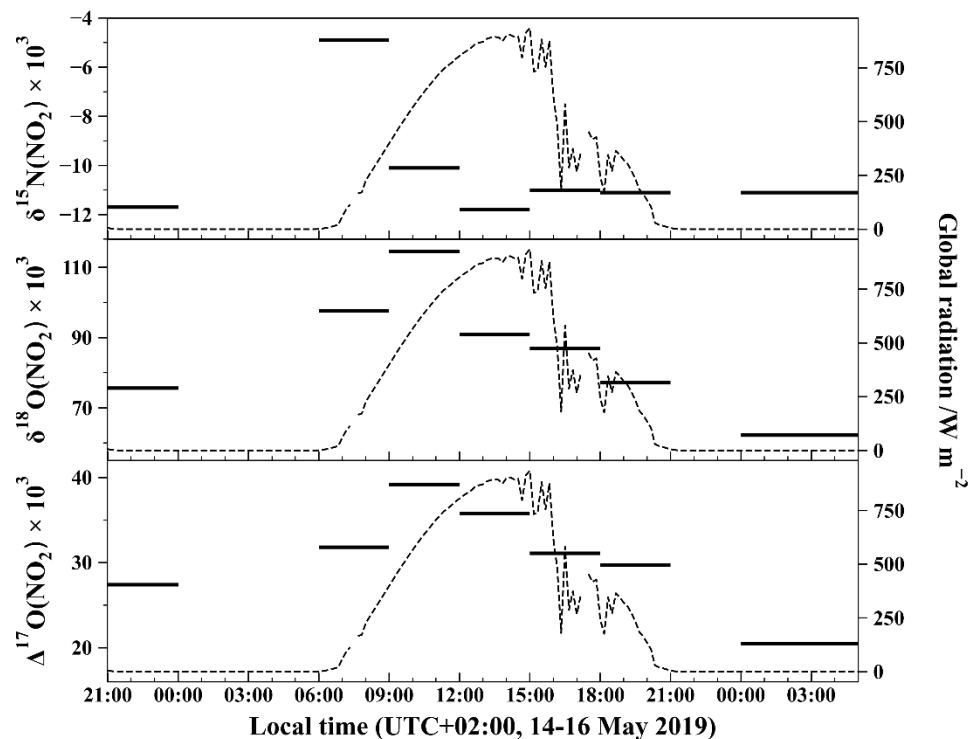


Figure 3. Temporal evolution of $\delta^{15}\text{N}$, $\delta^{18}\text{O}$ and, $\Delta^{17}\text{O}$ of atmospheric NO₂ measured with the azide method. Isotopic values for each 3 hours slots are from the same NO₂ sample collected over 3 hours (except for the last period which lasted 5 hours). Global solar radiation flux is represented by dashed lines (measured at 200 meters from the sampling site by the IGE weather station with a Skye SP1110 pyranometer).

4.1 Oxygen isotope composition

The time evolution of $\delta^{18}\text{O}$ of atmospheric NO₂ ($\delta^{18}\text{O}(\text{NO}_2)$) shown in Fig. 3 exhibits a substantial diurnal variation with a day mean of $(93.4 \pm 13.9) \text{ ‰}$ and a night mean of $(68.9 \pm 9.5) \text{ ‰}$. A maximum value of 114.5 ‰ is observed in the morning (09:00-12:00 interval) and a minimum value of 62.2 ‰ for the late-night interval (00:00-05:00). Using a similar sampling apparatus

245 during summer in the urban/sub-urban site of West Lafayette, USA, Walters et al. (2018) reported daytime and nighttime mean $\delta^{18}\text{O}(\text{NO}_2)$ values of $(86.5 \pm 14.1) \text{ ‰}$ and $(56.3 \pm 7.1) \text{ ‰}$, respectively. Although our daytime values are higher than those of

250 Walters et al. (2018), both datasets exhibit the same day-night contrast with a maximum during the day and a minimum at night. As expected from $\delta^{18}\text{O}$ values, $\Delta^{17}\text{O}(\text{NO}_2)$ follows a similar diurnal variation with a maximum value of 39.2 ‰ for the 09:00-12:00 interval and a minimum value of 20.5 ‰ for the 00:00-05:00 interval. High $\Delta^{17}\text{O}$ values are expected to reflect

255 the importance of ozone in the oxidation of NO to NO₂. Since daytime and nighttime chemistries are radically different, interpretations of our $\Delta^{17}\text{O}$ measurements and their implications are discussed separately by day and night.

4.1.1 Fundamentals of NO_x chemistry and isotopic transfers

NO_x are mainly produced under the form of NO by combustion and lighting processes (Dennison et al., 2006; Young, 2002) and by the biological activity of soils (Davidson and Kingerlee, 1997). In the daytime, NO and NO₂ rapidly interconvert in a

255 time scale of about 1-2 minutes establishing a photostationary steady state (PSS; Leighton 1961):



This so-called null cycle can be disturbed by RO₂ radicals when NO_x mixing ratios are relatively high, typically above 30-100

260 pmol mol⁻¹ (Seinfeld and Pandis, 2006; Monks, 2005):



The reaction between NO and RO₂ competes with the NO + O₃ reaction, allowing NO₂ formation without the consumption of an ozone molecule in the cycle (Monks, 2005). This results in ozone production and can lead to severe ozone build up in polluted areas. At night, RO₂ mixing ratios are strongly reduced making ozone the main NO oxidant following R3.

265 NO_x are mainly removed from the atmosphere via the oxidation of NO₂ into nitric acid during the day:



and at night:



270 In this framework, $\Delta^{17}\text{O}(\text{NO}_2)$ is driven by the relative importance of the different NO_2 production channels because NO_2 loss processes do not fractionate in terms of oxygen mass-independent anomaly. Each NO_2 production channel generates a specific mass-independent isotopic anomaly $\Delta^{17}\text{O}$ on the produced NO_2 (Kaiser et al., 2004). Based on the NO_2 continuity equation, this can be expressed with the following $\Delta^{17}\text{O}(\text{NO}_2)$ mass-balance equation (Morin et al., 2011):

$$\frac{d}{dt}([\text{NO}_2] \times \Delta^{17}\text{O}(\text{NO}_2)) = \sum_i (P_i \times \Delta^{17}\text{O}_i(\text{NO}_2)) - (\sum_j L_j) \times \Delta^{17}\text{O}(\text{NO}_2) \quad (2)$$

275 with $[\text{NO}_2]$ being the atmospheric NO_2 mixing ratio, P_i and L_j the NO_2 production/emission and loss rates (= mixing ratio of involved species multiplied by the kinetic constant of the considered chemical reaction), and $\Delta^{17}\text{O}_i(\text{NO}_2)$ the specific isotope anomaly transferred to NO_2 through the production reaction i .

4.1.2 $\Delta^{17}\text{O}_{\text{day}}(\text{NO}_2)$

By day, the NO_x photochemical cycle (R1 to R4) achieves a steady state in 1-2 minutes, which is several orders of magnitude faster than NO_2 loss reactions (Atkinson et al., 1997) and emission rate (NO_x are mainly emitted under the form of NO ; Villena et al., 2011). It follows that NO and NO_2 short variations can be neglected i.e. $\frac{d}{dt}[\text{NO}_2] \approx 0$ and $\frac{d}{dt}[\text{NO}] \approx 0$ on short timescales. In addition, fast interconversions between NO and NO_2 generate quickly an isotopic equilibrium between NO and NO_2 resulting in $\Delta^{17}\text{O}(\text{NO}_2) \approx \Delta^{17}\text{O}(\text{NO})$ (Michalski et al., 2014; Morin et al., 2007). With these approximations, considering only the main reactions and neglecting halogen chemistry, Eq.(2) yields to (Morin et al., 2007):

$$285 \Delta^{17}\text{O}_{\text{day}}(\text{NO}_2) \approx \frac{k_{\text{NO}+\text{O}_3}[\text{O}_3] \times \Delta^{17}\text{O}_{\text{NO}+\text{O}_3}(\text{NO}_2) + k_{\text{NO}+\text{RO}_2}[\text{RO}_2] \times \Delta^{17}\text{O}_{\text{NO}+\text{RO}_2}(\text{NO}_2)}{k_{\text{NO}+\text{O}_3}[\text{O}_3] + k_{\text{NO}+\text{RO}_2}[\text{RO}_2]} \quad (3)$$

with $\Delta^{17}\text{O}_{\text{NO}+\text{O}_3}(\text{NO}_2)$ being the ozone isotopic anomaly transferred to NO during its oxidation to NO_2 via R3 (also called the transfer function of the isotope anomaly of ozone to NO_2 ; Savarino et al., 2008) and $\Delta^{17}\text{O}_{\text{NO}+\text{RO}_2}(\text{NO}_2)$ being the RO_2 isotopic anomaly transferred to NO during its oxidation to NO_2 via R4. $\Delta^{17}\text{O}_{\text{NO}+\text{RO}_2}(\text{NO}_2)$ can be considered to be negligible (Alexander et al., 2020; Michalski et al., 2003) because RO_2 are mainly formed by the reactions $\text{R} + \text{O}_2$ and $\text{H} + \text{O}_2$ and the isotopic anomaly of atmospheric O_2 is very close to 0 ‰ (Barkan and Luz, 2003). This assumption has been estimated to affect the overall $\Delta^{17}\text{O}$ of RO_2 values by less than 1 ‰ (Röckmann et al., 2001). As a result, Eq.(3) can be simplified, giving a $\Delta^{17}\text{O}_{\text{day}}(\text{NO}_2)$ driven by the relative importance of R3 ($\text{NO} + \text{O}_3$) and R4 ($\text{NO} + \text{RO}_2$) in the NO oxidation and by the oxygen isotopic anomaly transferred from O_3 to NO_2 :

$$\Delta^{17}\text{O}_{\text{day}}(\text{NO}_2) \approx T_{\text{NO}+\text{O}_3} \times \Delta^{17}\text{O}_{\text{NO}+\text{O}_3}(\text{NO}_2) \quad (4)$$

295 with $T_{\text{NO+O}_3} = \frac{k_{\text{NO+O}_3}[\text{O}_3]}{k_{\text{NO+O}_3}[\text{O}_3] + k_{\text{NO+RO}_2}[\text{RO}_2]}$ (5)

$\Delta^{17}\text{O}_{\text{NO+O}_3}(\text{NO}_2)$ has been determined experimentally by Savarino et al. (2008). They reported $\Delta^{17}\text{O}_{\text{NO+O}_3}(\text{NO}_2) = 1.18 \pm 0.07 \times \Delta^{17}\text{O}(\text{O}_3) + (6.6 \pm 1.5) \text{‰}$ with $\Delta^{17}\text{O}(\text{O}_3)$ being the bulk ozone isotopic anomaly. $\Delta^{17}\text{O}(\text{O}_3)$ has been measured in Grenoble in 2012 (Vicars and Savarino, 2014) with a mean value of $(26.2 \pm 1.3) \text{‰}$, corresponding to a $\Delta^{17}\text{O}_{\text{NO+O}_3}(\text{NO}_2)$ value of $(37.5 \pm 2.8) \text{‰}$ which, according to Eq.(4), would give a maximum $\Delta^{17}\text{O}_{\text{day}}(\text{NO}_2)$ value of $(37.5 \pm 2.8) \text{‰}$. It is consistent with our maximum measured $\Delta^{17}\text{O}(\text{NO}_2)$ value of 39.2‰ for the 09:00-12:00 interval. In light of the known uncertainties, the small difference is not significant and is much smaller than the diurnal variations of $\Delta^{17}\text{O}(\text{NO}_2)$. Note that the $\Delta^{17}\text{O}$ calibration is not very accurate for the most enriched samples because nitrite standards with high $\Delta^{17}\text{O}$ are still not readily available. In a laboratory study Michalski et al. (2014) measured the $\Delta^{17}\text{O}$ of NO_2 formed by the photochemical $\text{NO}-\text{NO}_2-\text{O}_3$ cycle and reported $\Delta^{17}\text{O}(\text{NO}_2) = (39.3 \pm 1.9) \text{‰}$. Despite experimental conditions that are not strictly applicable to our atmospheric conditions (e.g. $\text{NO}_x \gg \text{O}_3$, light source, absence of VOCs), their value is surprisingly close to our maximum value. Assuming that our maximum $\Delta^{17}\text{O}(\text{NO}_2)$ value correspond to $T_{\text{NO+O}_3}$ close to unity ($\text{R3}(\text{NO} + \text{O}_3) \gg \text{R4}(\text{NO} + \text{RO}_2)$), we use a $\Delta^{17}\text{O}_{\text{NO+O}_3}(\text{NO}_2)$ value of 39.2‰ for the following calculations. Combining Eq.(4) and Eq.(5), an expression for the RO_2 mixing ratio can be derived as:

$$[\text{RO}_2] = \frac{k_{\text{NO+O}_3}[\text{O}_3]}{k_{\text{NO+RO}_2}} \left(\frac{\Delta^{17}\text{O}_{\text{NO+O}_3}(\text{NO}_2)}{\Delta^{17}\text{O}_{\text{day}}(\text{NO}_2)} - 1 \right) \quad (6)$$

310 Figure 4 shows the daytime evolution of $T_{\text{NO+O}_3}$ calculated from Eq.(4) and RO_2 calculated from Eq.(6). $T_{\text{NO+O}_3}$ varies between 0.76 and 1 with a mean daytime of 0.86 (the measured daytime $\Delta^{17}\text{O}(\text{NO}_2)$ mean value is $(33.5 \pm 3.9) \text{‰}$) meaning that 86 % of NO_2 is formed via R3 (oxidation of NO by O_3). The mean estimated RO_2 mixing ratio is $(13.8 \pm 11.2) \text{ pmol mol}^{-1}$. Note that $\text{RO}_2 = 0 \text{ pmol mol}^{-1}$ for the 09:00-12:00 interval originates from our assumption of $T_{\text{NO+O}_3} = 1$ for our highest $\Delta^{17}\text{O}(\text{NO}_2)$ value; in reality, it only means that RO_2 is so low that $\text{R3}(\text{NO} + \text{O}_3) \gg \text{R4}(\text{NO} + \text{RO}_2)$. Overall, our RO_2 values are found to 315 be within the range of values measured at urban/peri-urban sites (see Table 2). However, RO_2 diurnal variation at our site does not follow the pattern of previous measurements which usually report a diurnal variation with a maximum varying from noon to early afternoon (Fuchs et al., 2008; Tan et al., 2017) whereas this study shows a maximal mixing ratio in late afternoon. With such a limited dataset (only 1 day of sampling), it is not possible to draw general conclusions on the NO_x/RO_2 chemistry 320 dynamics. An important recommendation for further investigation is to conduct isotopic measurements with accurate measurements of key atmospheric radicals/oxidants, e.g. NO , O_3 , and possibly RO_2 , in order to test quantitatively our isotopic approach. Additionally, the use of a chemical box-model is also recommended because it would allow to account for non-equilibrium effects in isotopic transfers and thus strengthen the interpretation of isotopic measurements in the investigation of the reactive nitrogen cycle in urban atmospheres.

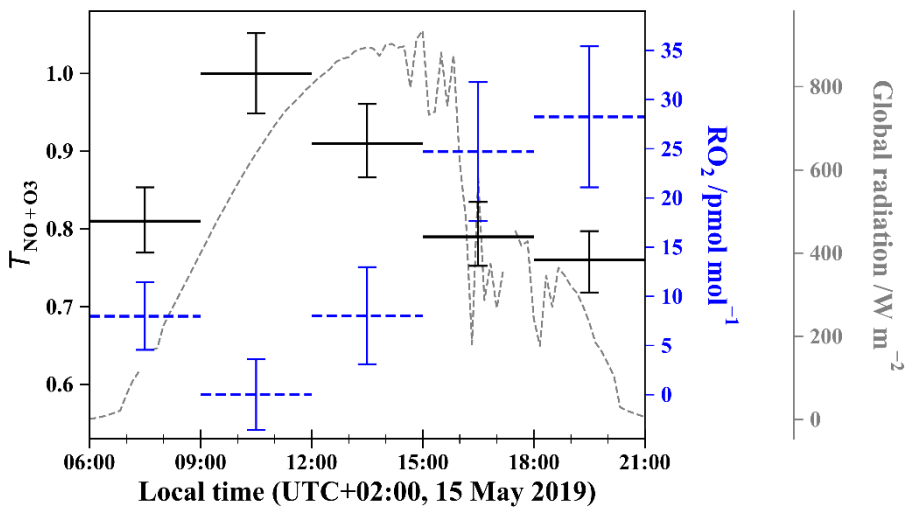


Figure 4. Daytime evolution of $T_{\text{NO}+\text{O}_3}$ (solid black line with error bars) estimated from Eq.(4) using measured $\Delta^{17}\text{O}(\text{NO}_2)$ in Grenoble, and of RO_2 mixing ratios (dashed blue line with error bars) estimated from Eq.(6). Error bars for $T_{\text{NO}+\text{O}_3}$ are derived from standard deviations of $\Delta^{17}\text{O}(\text{NO}_2)$ and $\Delta^{17}\text{O}(\text{O}_3^*)$ measured in Grenoble (Vicars and Savarino, 2014). RO_2 error bars are derived from O_3 measurement uncertainties and errors on $T_{\text{NO}+\text{O}_3}$ (by comparison, errors on reaction constants can be neglected). Global solar radiation flux is represented by dashed lines (measured at 200 meters from the sampling site by the IGE weather station with a Skye SP1110 pyranometer).

Site	$\text{RO}_2 / \text{pmol mol}^{-1}$	Reference
Grenoble (2019, May)	0-35 ^(*)	This study
UK, suburban site (2003, July-August)	4-22	Emmerson et al. (2007)
Germany, suburban site (2005, July)	2-40	Fuchs et al. (2008)
Germany, rural site (1998, July-August)	2-50	Mihelcic et al. (2003)
USA, rural site (2002, May-June)	9-15	Ren et al. (2005)
China, rural site (2014, June-July)	7-37	Tan et al. (2017)

Table 2. Mean daytime RO_2 mixing ratios ranges measured during field campaigns in various environments and seasons. ^(*)Derived from Eq.(6) using $\Delta^{17}\text{O}$ values of atmospheric NO_2 in Grenoble.

Morin et al. (2011) simulated the diurnal variation of $\Delta^{17}\text{O}(\text{NO}_2)$ in a remote marine boundary layer without the effect of NO_x emissions. They assumed $\Delta^{17}\text{O}(\text{O}_3) = 30 \text{ ‰}$ ($\Delta^{17}\text{O}_{\text{NO}+\text{O}_3}(\text{NO}_2) = 45 \text{ ‰}$) resulting into higher overall $\Delta^{17}\text{O}(\text{NO}_2)$ values compared to our study. Their simulated $\Delta^{17}\text{O}(\text{NO}_2)$ exhibited large diurnal variations with maximum values at night (close to 41 ‰) and minimum values at noon of 28 ‰. This is consistent with RO_2 mixing ratio reaching a maximum around local noon

in clean environments. In contrast to their model simulations, our daytime $\Delta^{17}\text{O}(\text{NO}_2)$ measurements are higher than our nighttime measurements. We will show in the following section that this difference originates from absence of NO_x emissions in Morin et al. (2011) photochemical modelling.

4.1.3 $\Delta^{17}\text{O}_{\text{night}}(\text{NO}_2)$

350 Without photolysis at night and associated RO_2 production, ozone is the unique NO oxidant. NO and NO_2 are no longer in photochemical equilibrium because NO_2 cannot be converted back into NO. As a result, the oxygen isotopic composition of NO_2 formed during the night is determined by the oxygen isotopic composition of O_3 and emitted NO. Additionally, in order to estimate the overall isotopic signature of sampled NO_2 at night, we need to determine the residuals of NO_2 formed during the day that is still present during the night, following:

$$355 \quad \Delta^{17}\text{O}_{\text{night}}(\text{NO}_2) \approx x \times \Delta^{17}\text{O}_{\text{day}}(\text{NO}_2) + \frac{(1-x)}{2} \times (\Delta^{17}\text{O}_{\text{NO+O}_3}(\text{NO}_2) + \Delta^{17}\text{O}(\text{NO})) \quad (7)$$

with x being the fraction of NO_2 formed during the day to the total NO_2 measured at night and $(1-x)$ representing the fraction of NO_2 which has been produced during the night to the total NO_2 measured at night. NO is mainly emitted by combustion processes in which a nitrogen atom (from atmospheric N_2 or N present in fuel) is added to an oxygen atom formed by the thermal decomposition of O_2 (Zeldovich, 1946). With $\Delta^{17}\text{O}(\text{O}_2)$ being close to 0 ‰ (Barkan and Luz, 2003), NO emissions are

360 very likely to have a $\Delta^{17}\text{O} \approx 0$ ‰, or at least negligible compared to $\Delta^{17}\text{O}_{\text{NO+O}_3}(\text{NO}_2)$. Using Eq.(7) and assuming a negligible isotope anomaly for NO, the time evolution of $\Delta^{17}\text{O}(\text{NO}_2)$ over the night can be calculated. It is worth pointing out that the x fraction becomes very small at the end of the night allowing to further simplify Eq.(7): $\Delta^{17}\text{O}_{\text{night}}(\text{NO}_2) = \frac{1}{2} \times \Delta^{17}\text{O}_{\text{NO+O}_3}(\text{NO}_2)$. Thus, if there are nighttime NO emissions, a measurement of $\Delta^{17}\text{O}(\text{NO}_2)$ at the end of the night is also an interesting way of deriving $\Delta^{17}\text{O}(\text{O}_3)$ which is difficult to measure directly. The nighttime variation of the x fraction is
365 estimated considering that the nighttime lifetime of NO_2 relative to oxidation via ozone and dry deposition is 7.2 hours (O_3 chemical sink is dominant over deposition by a factor $> 10^4$ with $k_{\text{NO}_2+\text{O}_3} = 1.4 \times 10^{-13} \exp[-2470(\text{K})/\text{T}] \text{ cm}^3 \text{ mol}^{-1} \text{ s}^{-1}$ Atkinson et al., 2004; NO_2 dry velocity $V_d = 0.25 \text{ cm s}^{-1}$ Holland et al., 1999 and assuming a nighttime boundary layer height of 500 m). For the 00:00-05:00 interval, we calculate a mean value of $\Delta^{17}\text{O}(\text{NO}_2) = 19.9$ ‰ (with an overall error of about 1.6 ‰) which is very close to our measured $\Delta^{17}\text{O}(\text{NO}_2)$ of 20.5 ‰. This first dataset of nighttime $\Delta^{17}\text{O}(\text{NO}_2)$ measurements appears to
370 confirm our understanding of nocturnal NO_2 formation (Alexander et al., 2020; Michalski et al., 2014). NO emissions in urban areas have a very significant influence on $\Delta^{17}\text{O}(\text{NO}_2)$ leading to a behaviour in opposition to the one observed in remote locations. As illustrated by Morin et al. (2011), $\Delta^{17}\text{O}(\text{NO}_2)$ is predicted to be maximal at night in remote areas where NO emissions are negligible, reflecting the isotopic signature of NO_2 at sunset. In areas where nighttime NO emissions are high, nighttime $\Delta^{17}\text{O}(\text{NO}_2)$ can be up to a factor of two smaller than in remote areas.

375 **4.2 Nitrogen isotope composition**

Measured $\delta^{15}\text{N}(\text{NO}_2)$ values range from -11.8 to -4.9 ‰ with no clear diurnal variation and values clustering around an overall mean of $(-10.2 \pm 2.2)\text{ ‰}$ (see Fig. 3). Using a similar method, Walters et al. (2018) collected atmospheric NO_2 over one month in a urban/sub-urban location during the summer. They reported a mean $\delta^{15}\text{N}$ value of $(-11.4 \pm 6.9)\text{ ‰}$, very close to our mean value but with a wider overall range (from -31.4 to $+0.4\text{ ‰}$). In another urban area but using passive samplers, Dahal and Hastings (2016) reported mean $\delta^{15}\text{N}(\text{NO}_2)$ values of $(-8.3 \pm 0.9)\text{ ‰}$ and $(-6.4 \pm 1.4)\text{ ‰}$ for summer and winter periods, respectively. All these values are within the $\delta^{15}\text{N}$ range for NO emitted by industrial combustion and traffic sources which are reported to vary from -19.7 to -13.7 ‰ and from -9 to -2 ‰ respectively (Miller et al., 2017; Walters et al., 2015). Interestingly, all the $\delta^{15}\text{N}$ values measured at our sampling site fall within a narrow range, from about -12 to -10 ‰ , except for the sample collected between 06:00 and 09:00 which has a much higher value of -4.9 ‰ . This singular value is well correlated with the morning NO traffic emission spike (see Fig. 2). However, once emitted into the atmosphere, NO can undergo isotopic fractionations that modify the nitrogen isotope distribution in NO_2 relative to emitted NO (Freyer et al., 1993). In order to use $\delta^{15}\text{N}(\text{NO}_2)$ as a tracer of NO_x sources, we need to quantify these nitrogen isotopic shifts to correct measured $\delta^{15}\text{N}(\text{NO}_2)$. Nitrogen isotopic fractionation, defined as $\Delta(\text{NO}_2 - \text{NO}_x) = \delta^{15}\text{N}(\text{NO}_2) - \delta^{15}\text{N}(\text{NO}_x)$, is the result of a combination of three effects: 1) an Equilibrium Isotope Effect (EIE) between NO and NO_2 and 2) a Kinetic Isotope Effect (KIE) during NO oxidation to NO_2 and 3) a Photochemical Isotope Fractionation Effect (PHIFE) during NO_2 photolysis (other NO_2 sinks are negligible during the day). The overall daytime nitrogen isotopic shift of NO_2 relative to emitted NO_x ($\Delta_{\text{day}}(\text{NO}_2 - \text{NO}_x)$) can be estimated using the steady-state isotopic mass balance for NO_2 . Li et al. (2020) derived an expression for $\Delta(\text{NO}_2 - \text{NO}_x)$ assuming that the conversion of NO to NO_2 is solely driven by O_3 . This could therefore lead to uncertainties on the NO_2 shift when other conversion pathways become significant with respect to the NO conversion by O_3 . A more general expression for $\Delta(\text{NO}_2 - \text{NO}_x)$ can be derived taking into account the conversion of NO to NO_2 via other species, notably RO_2 (see equation C11 in appendix C). In our urban environment, we only consider the conversion of NO into NO_2 via O_3 and RO_2 during the day. Assuming $\alpha_{\text{KIE}(\text{NO}+\text{O}_3)} \approx \alpha_{\text{KIE}(\text{NO}+\text{RO}_2)}$ (see derivation in appendix C), $\Delta_{\text{day}}(\text{NO}_2 - \text{NO}_x)$ can be expressed by

$$\Delta_{\text{day}}(\text{NO}_2 - \text{NO}_x) = \frac{\alpha_{\text{LCIE}} * A^*_{\text{day}} + (\alpha_{\text{EIE}} - 1)}{A^*_{\text{day}} + 1} (1 - f_{\text{NO}_2}) \quad (8)$$

400 with $\alpha_{\text{LCIE}} * = \alpha_{\text{KIE}(\text{NO}+\text{O}_3)} - \alpha_{\text{PHIFE}}$

$$\text{and } A^*_{\text{day}} = \frac{J_{\text{NO}_2}}{k_{\text{NO}+\text{NO}_2} [\text{NO}]} = \frac{k_{\text{NO}+\text{O}_3} [\text{O}_3] + k_{\text{NO}+\text{RO}_2} [\text{RO}_2]}{k_{\text{NO}+\text{NO}_2} [\text{NO}_2]}$$

where $f_{\text{NO}_2} = [\text{NO}_2]/[\text{NO}_x]$, α_{LCIE}^* the fractionation factor of combined KIE and PHIFE and α_{EIE} the EIE fractionation factor. A^*_{day} is defined as the ratio of the NO_2 lifetime with respect to isotopic exchanges over the daytime NO_2 chemistry lifetime.

J_{NO_2} is the NO_2 photolysis rate, $k_{\text{NO}+\text{O}_3}$ is the rate constant of reaction $\text{NO} + \text{O}_3$, $k_{\text{NO}+\text{RO}_2}$ is the rate constant of reaction $\text{NO} + \text{RO}_2$ and $k_{\text{NO}+\text{NO}_2}$ is the rate constant of the isotopic exchange (CR1) (see Appendix D for rate constants data). Interestingly, we can combine Eq.(8) and Eq.(6), and express A^*_{day} as a function of oxygen isotopic variables discussed in the previous section:

$$A^*_{\text{day}} = \frac{k_{\text{NO}+\text{O}_3}[\text{O}_3]}{k_{\text{NO}+\text{NO}_2}[\text{NO}_2]} \left(\frac{\Delta^{17}\text{O}_{\text{NO}+\text{O}_3}(\text{NO}_2)}{\Delta^{17}\text{O}_{\text{day}}(\text{NO}_2)} \right) \quad (9)$$

Since our NO measurements are not precise and we do not have direct measurements of J_{NO_2} or RO_2 , we use Eq.(9) to estimate

410 the NO_2 isotopic fractionation shift. Note that, although Li et al. (2020) only consider the NO conversion via O_3 in the analysis of their nitrogen isotopic data, they found an excellent agreement between their calculated values and field isotopic measurements at Jülich, Germany (Freyer et al., 1993). Nonetheless, the reason of this accordance remains unclear, as it could be attributable to an equivalent KIE of $\text{NO} + \text{O}_3$ and $\text{NO} + \text{RO}_2$ but also to the dominance of the NO oxidation via O_3 over RO_2 .

415 At night, the isotopic fractionation shift $\Delta_{\text{night}}(\text{NO}_2 - \text{NO}_x)$ is driven by EIE, KIE, the N isotopic composition of NO emissions, and f_{NO_2} , given that J_{NO_2} is null (see derivation in appendix C):

$$\Delta_{\text{night}}(\text{NO}_2 - \text{NO}_x) \approx \frac{A^*_{\text{night}} \left(\alpha_{\text{KIE}} - \left(\frac{1 + \delta^{15}\text{N}(\text{NO}_{\text{emis}})}{1 + \delta^{15}\text{N}(\text{NO}_2)} \right) \right) + (\alpha_{\text{EIE}} - 1)}{A^*_{\text{night}} + 1} (1 - f_{\text{NO}_2}) \quad (10)$$

where $\delta^{15}\text{N}(\text{NO}_{\text{emis}})$ is the N isotopic composition of NO emissions

$$\text{and } A^*_{\text{night}} = \frac{k_{\text{NO}+\text{O}_3}[\text{O}_3]}{k_{\text{NO}+\text{NO}_2}[\text{NO}_2]} = \frac{E(\text{NO})}{k_{\text{NO}+\text{NO}_2}[\text{NO}][\text{NO}_2]} \quad (11)$$

420 with $E(\text{NO})$ the NO emission flux. From laboratory experiments, Li et al. (2020) reported fractionation factors of 1.0289 ± 0.0019 and 0.990 ± 0.005 , for α_{EIE} and α_{LCIE} , respectively. Using these experimental values and the ambient mixing ratios of ozone, NO and, NO_2 measured at our sampling site, we estimate the time evolution of $\Delta(\text{NO}_2 - \text{NO}_x)$ from Eq.(8) and Eq.(9) for daytime. At night, $[\text{NO}] \ll [\text{NO}_2]$ and hence f_{NO_2} tends towards 1 and $\Delta_{\text{night}}(\text{NO}_2 - \text{NO}_x) \approx 0$ (Table 3 provides the calculated values). $\Delta(\text{NO}_2 - \text{NO}_x)$ values are found to be negligible during the entire sampling period except between 06:00 and 09:00 with a mean $\Delta(\text{NO}_2 - \text{NO}_x)$ value of 2.7 ‰ due to lower f_{NO_2} and A^*_{day} values. Overall, in our moderately polluted environment, nitrogen oxide isotope effects appear to induce very small nitrogen isotopic shift, reflecting the fact that NO_x is overwhelmingly under the form of NO_2 (mean $f_{\text{NO}_2} = 0.93$). Our results are in good agreement with the $\Delta(\text{NO}_2 - \text{NO}_x)$ range (between 1.3 and 2.5 ‰) calculated from isotopic measurements at West Lafayette, USA (Walters et al., 2018). Moreover, Li

et al. (2020) calculated a mean $\Delta(\text{NO}_2 - \text{NO}_x)$ of $(1.3 \pm 3.2) \text{ ‰}$ from isotopic measurements near San Diego, USA (NO_x

430 mixing ratios varied from 1 to 9 nmol mol⁻¹).

Sampling date & time (start - end)	f_{NO_2}	A^*	$\Delta(\text{NO}_2 - \text{NO}_x) / \text{‰}$	$\delta^{15}\text{N}(\text{NO}_x) / \text{‰}$
14 May 2019 21:00 - 00:00	1.00	1.70	0.00	-11.70
15 May 2019 06:00 - 09:00	0.87	0.27	2.72	-7.62
15 May 2019 09:00 - 12:00	0.85	1.46	0.85	-10.95
15 May 2019 12:00 - 15:00	0.81	2.61	0.01	-11.81
15 May 2019 15:00 - 18:00	0.95	3.38	-0.13	-10.87
15 May 2019 18:00 - 21:00	1.00	3.04	0.00	-11.22
16 May 2019 00:00 - 05:00	1.00	0.42	0.00	-11.10

Table 3. Summary of measured f_{NO_2} , calculated A^* values using Eq.(9) for daytime and Eq.(11) for nighttime, calculated isotopic fractionation between NO_2 and NO_x ($\Delta(\text{NO}_2 - \text{NO}_x)$) using Eq.(8) for daytime, and Eq.(10) for nighttime and, $\delta^{15}\text{N}(\text{NO}_x)$ estimated with $\Delta(\text{NO}_2 - \text{NO}_x)$ and measured $\delta^{15}\text{N}(\text{NO}_2)$.

Using estimated $\delta^{15}\text{N}(\text{NO}_x)$, we evaluate the relative contributions of the dominant NO_x sources at our site using the Bayesian

isotopic mixing model SIAR (Stable Isotope Analysis in R; Parnell et al., 2010). Initially developed for ecological studies (Inger et al., 2006; Samelius et al., 2007), isotopic mixing models have been recently used for atmospheric applications, notably

435 to identify major NO_x sources of aerosol nitrate from $\delta^{15}\text{N}$ (Jin et al., 2021; Zong et al., 2017; Fan et al., 2019). Using as inputs not only isotopic measurements but also their uncertainties, the SIAR model can be used to calculate potential NO_x sources solutions as probability distributions. A recent emission inventory of NO_x in the Grenoble urban area estimated that, in 2016, 52 % of emitted NO_x could be attributed to transport, 26 % to industries, 20% to the residential/tertiary sectors and, 2 % to agriculture (Topin et al., 2019). Looking at the type of energy consumed by each sector, we estimate that at this time of the 440 year, our sampling site was mostly influenced by fossil-fuel combustion NO_x sources, mainly gasoline/diesel and natural-gas, and by biogenic NO_x sources (soils emissions). As shown by previous studies, $\delta^{15}\text{N}$ of NO_x emitted by vehicle exhausts depends on the fuel type, the reduction emission technology, and the vehicle run time with values ranging from -21 ‰ to -2 ‰ (Walters et al., 2015). As 90 % of traffic- NO_x are emitted by diesel-powered engines in the Grenoble urban area (Atmo-Auvergne-Rhônes-Alpes, 2018), we use a value of $(-4.7 \pm 1.7) \text{ ‰}$, representative of the U.S. vehicle fleet (Miller et al., 2017) 445 for which about 80 % of its traffic- NO_x emissions originate from diesel vehicles (Dallmann et al., 2013). For $\delta^{15}\text{N}$ of NO_x emitted by natural gas combustion, we use a value of $(-16.5 \pm 1.7) \text{ ‰}$ which is the average isotopic signature of natural gas-burning power plants and residential furnace exhausts (Walters et al., 2015). Despite the large range of $\delta^{15}\text{N}$ values for biogenic 450 NO_x , (from -59.8 to -19.9 ‰) (Li and Wang, 2008; Yu and Elliott, 2017; Walters et al., 2015), these values are still very distinct from $\delta^{15}\text{N}$ of fossil-fuel combustion NO_x , making possible to roughly estimate the relative contributions of different NO_x sources at our sampling site. We use a soil- NO_x $\delta^{15}\text{N}$ value of $(-33.8 \pm 12.2) \text{ ‰}$ (Zong et al., 2017) which is the average of values taken from several studies on NO_x emitted by natural and fertilized soil (Felix and Elliott, 2014; Li and Wang, 2008).

Over our sampling period, the SIAR model results indicate traffic as the dominant NO_x emission source with a mean relative contribution of $(57 \pm 8) \%$ (see Fig. 5). Natural gas combustion is found to be the second main NO_x emission source $(36 \pm 12) \%$ before soil emissions which account for only $(7 \pm 5) \%$. The limited nature of our measurement dataset (only one day of 455 sampling) prevents us to draw any general and robust conclusions on the relative contributions of NO_x emissions at our site. Nonetheless, we note that the SIAR overall source apportionment is in close agreement with the Grenoble urban area emission inventory concerning traffic emissions $(52 \% \text{ in 2016})$, lending some support to the idea that $\delta^{15}\text{N}$ of NO_2 is a reliable tracer of NO_x emission sources after correction for LCIE and EIE.

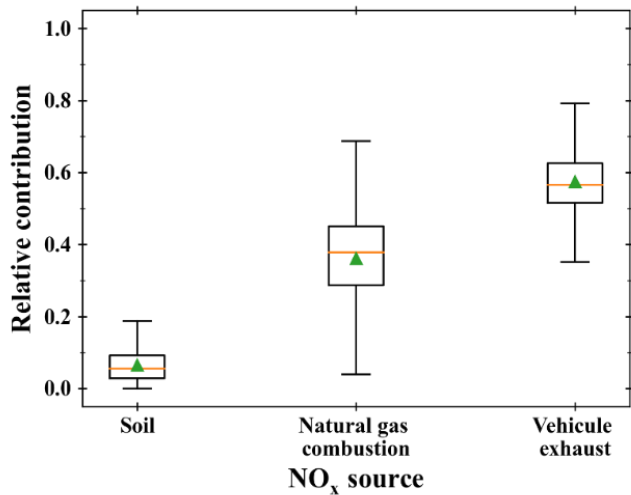


Figure 5. Potential NO_x emission source partitioning using the SIAR model based on estimated $\delta^{15}\text{N}(\text{NO}_x)$. Reference values for each source were taken from Miller et al. (2017), Walters et al. (2015) and, Zong et al. (2017).

460 5 Conclusion

The primary goal of this preliminary work was to address an efficient and portable sampling system for atmospheric NO_2 fitting with accurate isotopic analysis of double nitrogen and triple oxygen isotopes. First simultaneous measurements of the multi-isotopic composition ($\delta^{15}\text{N}$, $\delta^{18}\text{O}$, and $\Delta^{17}\text{O}$) of atmospheric NO_2 are reported here, notably at relatively high temporal resolution (3 h). Over the course of more than one day in the Grenoble urban/suburban environment, $\Delta^{17}\text{O}(\text{NO}_2)$ is found to 465 vary diurnally with a maximum value of $(39.2 \pm 0.3) \text{ ‰}$ during the day and a minimum value of $(20.5 \pm 0.3) \text{ ‰}$ at night. At photo-stationary state, high $\Delta^{17}\text{O}(\text{NO}_2)$ values result from the ozone predominance in NO oxidation pathways whereas lower values reflect the influence of peroxy radicals. We estimate from our $\Delta^{17}\text{O}(\text{NO}_2)$ measurements that 86 % of NO_2 produced by day originates from the oxidation of NO by O_3 . Moreover, a mean daytime peroxy radical mixing ratio of $(13.8 \pm 11.2) \text{ pmol}$

mol⁻¹ is derived from the oxygen isotopic measurements. At night, NO_x photochemistry shutdowns and hence $\Delta^{17}\text{O}(\text{NO}_2)$ 470 decreases under the growing influence of the isotopic footprint from NO emitted by night. The $\Delta^{17}\text{O}(\text{NO}_2)$ measurement towards the end of the night is found to be quantitatively consistent with typical values of $\Delta^{17}\text{O}(\text{O}_3)$. The $\delta^{15}\text{N}(\text{NO}_2)$ measurements show little variations, from -11.8 to -4.9 ‰, with mostly negligible N isotope fractionations between NO and NO₂ due to the high NO₂/NO_x ratios. After correction of nitrogen isotopic fractionations, we use a Bayesian isotope mixing model to estimate the relative contributions of the dominant NO_x emissions sources. The results indicate the predominance of 475 traffic NO_x emissions in this area at (57 ± 8) %, before natural gas combustion and soil emission.

Despite the limited nature of our measurement dataset, our results shed light on the sensitivity of NO₂ isotopic signature to the atmospheric chemical regimes and emissions of the local environment. This isotopic approach can be applied to various environments in order to probe further the oxidative chemistry and help to constrain the NO_x fate in a more quantitative way. 480 In the future, the interpretation of the isotopic data should be extended with the use of a photochemical box model including isotopic anomaly transfers and local emissions in order to solve persistent issues of atmospheric oxidation mechanisms. Moreover, samplings and multi-isotopic analysis of atmospheric nitrate performed in parallel to those of NO₂ would certainly be of interest for the study of the full reactive nitrogen cycle.

Appendix A: Isotopic standards and calibration

This method of analysis induces isotope fractionations during NO₂⁻/N₂O conversion and ionization in the spectrometer, as well 485 as isotope exchanges between NO₂⁻ and its medium. Indeed, while isotope exchanges between nitrite and its matrix are minimized due to the basic pH, the chemistry required to convert nitrite to N₂O involves a step in an acidic medium that promotes an exchange of oxygen isotopes (Casotti et al., 2007). In order to eliminate the effects of these isotope splits, the system is calibrated using standards of known isotopic composition, which are subjected to the same treatment as the samples. This is called the identical treatment principle (Brand, 1996). By subjecting compounds of known isotopic composition to the 490 same treatment as the samples, the isotope fractionation induced by the analytical protocol can be estimated and the samples values can be corrected. Standards are first dissolved in a basic aqueous medium (pH = 12) and then, from this stock solution, five series of each standard are prepared in several amount ranges, namely, 40 nmol, 80 nmol, 100 nmol, 120 nmol and 150 nmol, in order to estimate the effects of the amount of a material on its isotopic measurement. The matrix used for their preparation is the same as that of the samples, i.e. a mixture of KOH 2 M/guaiacol in deionised water. Correction factors are 495 obtained by linear regression between the raw and the expected values of $\delta^{15}\text{N}$, $\delta^{18}\text{O}$ and $\delta^{17}\text{O}$ of the standards. Three international references of known $\delta^{15}\text{N}$ and $\delta^{18}\text{O}$ values are used for this work. These are nitrite salts, named RSIL-N7373, RSIL-N10219 and RSIL-N23 with respective $\delta^{15}\text{N}/\delta^{18}\text{O}$ values of $-79.6/4.2$ ‰, $2.8/88.5$ ‰, and $3.7/11.4$ ‰. Although the three standards cover a wide range of isotopic composition in $\delta^{15}\text{N}$ and $\delta^{18}\text{O}$, they do not have an isotopic anomaly in ^{17}O . As we are not aware of any available international reference nitrite standards with a known ^{17}O anomaly, we are currently in the 500 process of manufacturing our own standards. As this step is still under development, and in order to be able to assess the

accuracy of our ^{17}O measurements of atmospheric NO_2 samples, we have estimated the isotope fractionation that ^{17}O undergoes during the analysis. RSIL-N7373 and RSIL-N23 standards have a $\Delta^{17}\text{O} = 0\text{ ‰}$ so we estimate their ^{17}O composition such that $\delta^{17}\text{O} = 0.52 \times \delta^{18}\text{O}$. For standard RSIL-N10219, we measure a negative $\Delta^{17}\text{O}$ around -7 ‰ . We therefore apply the mass independent relation such that $\delta^{17}\text{O}_{\text{std}}(\text{RSIL-N10219}) = \Delta^{17}\text{O}_{\text{raw}}(\text{RSIL-N10219}) + 0.5 \times \delta^{18}\text{O}_{\text{std}}(\text{RSIL-N10219})$.

505 The isotopic exchange of ^{18}O is estimated at 11 % for standards at 100 nmol (Fig. A1) which is in line with Kobayashi et al. (2020) who have estimated the degree of O isotope exchange in the azide method between H_2O and NO_2^- to $(10.8 \pm 0.3)\text{ ‰}$. The ^{15}N calibration curve allows us to ensure a good fractionation rate during the analysis. Indeed, given the 1:1 association of the nitrogen atoms of nitrite and azide, the theoretical value of the calibration slope must be 0.5. The slight deviation from our measured value can be attributed to a blank effect, estimated here at 2 % of the size of the standards (6 % for those at 40 510 nmol).

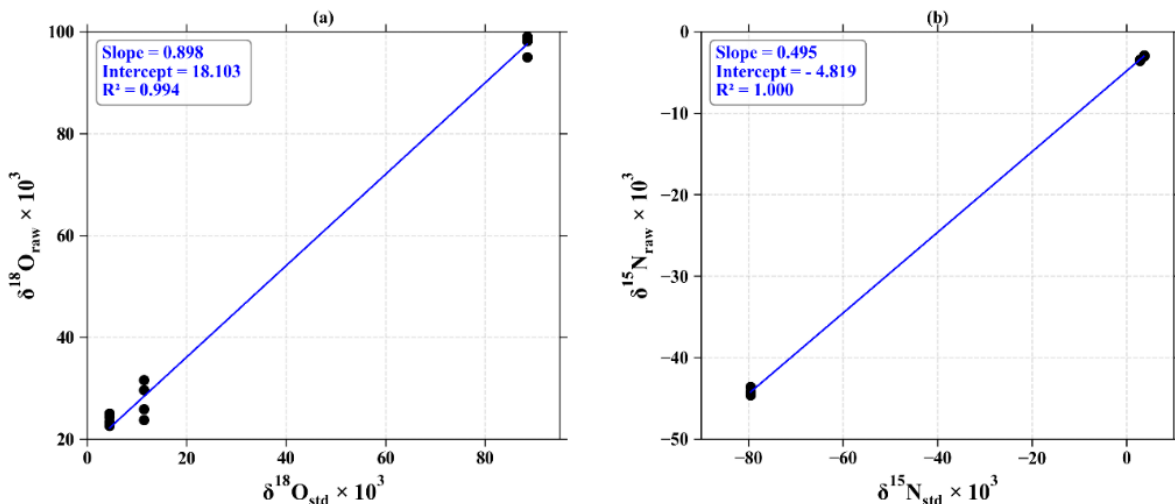


Figure A1. Calibration of (a) ^{18}O and (b) ^{15}N with nitrite standards at 100 nmol measured by the chemical azide method. The measured $\delta^{18}\text{O}$ ($\delta^{18}\text{O}_{\text{raw}}$) and $\delta^{15}\text{N}$ ($\delta^{15}\text{N}_{\text{raw}}$) values of NO_2^- standards are plotted against their certified reference $\delta^{18}\text{O}$ ($\delta^{18}\text{O}_{\text{std}}$) and $\delta^{15}\text{N}$ ($\delta^{15}\text{N}_{\text{std}}$) values.

Appendix B: Samples isotopic stability

Oxygen isotopes in nitrites are very labile (Böhlke et al., 2007) but the basic pH of the eluent limits isotopic exchanges. To ensure isotopic integrity from denuders extraction to analysis by IRMS, we followed Walters et al. (2018) procedure to quantify isotopic exchanges that might occur with the eluted matrix during storage. Thus, three solutions containing each 500 nmol of 515 a KNO_2 salt (RSIL-N7373, RSIL-N10219 and RSIL-N23) were prepared in the eluted matrix and kept frozen. We monitored the nitrite standards isotopic composition prepared in the eluted guaiacol matrix during 22 days. 100 nmol were collected from the individual solutions, analysed and refrozen until the next analysis. The temporal evolution of the $\delta^{17}\text{O}$, $\delta^{18}\text{O}$ and $\Delta^{17}\text{O}$

520 differences between our measurements of RSIL standards (prepared in the KOH/guaiacol eluted matrix) and their certified reference values is plotted in Fig. B1. It represents the temporal drift of the isotopic signal with respect to reference values. If
 525 the deviation is constant, it means that the isotopic signal is not degraded with time and its standard deviation is considered as the uncertainty in our $\delta^{17}\text{O}(\text{NO}_2)$ and $\delta^{18}\text{O}(\text{NO}_2)$ measurements. As shown in Fig. B1, deviation of the three standards was stable over the 22-days experiment with an overall mean of $(1.1 \pm 0.8) \text{ ‰}$, $(2.3 \pm 1.8) \text{ ‰}$, and $(-0.1 \pm 0.3) \text{ ‰}$ for $\delta^{17}\text{O}$, $\delta^{18}\text{O}$ and $\Delta^{17}\text{O}$, respectively. Note that RSIL-N10219 shows higher $\delta^{17}\text{O}$ and $\delta^{18}\text{O}$ residuals than the two other standards. The reason for this difference of behaviour is still not fully understood. As residuals remain steady over several weeks, we consider this method suitable for the oxygen analysis of NO_2 and the uncertainties applied to our isotopic measurements are reported as the propagation error of the mean measurement uncertainty and the mean uncertainty resulting from NO_2^- storage. In our study, average uncertainties on $\delta^{17}\text{O}$, $\delta^{18}\text{O}$, and $\Delta^{17}\text{O}$ are estimated to be ± 0.8 , ± 1.8 and, $\pm 0.3 \text{ ‰}$, respectively (1σ uncertainties).

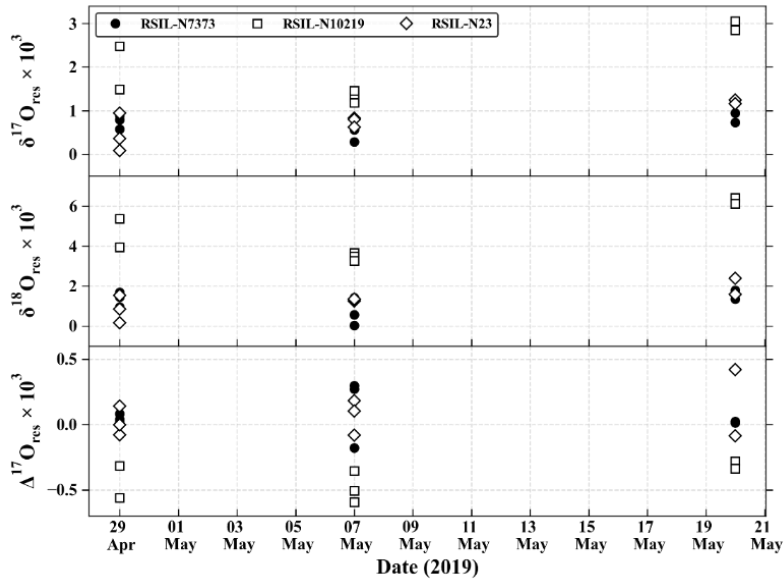


Figure B1. Temporal evolution of $\delta^{17}\text{O}$, $\delta^{18}\text{O}$ and, $\Delta^{17}\text{O}$ differences between our measurements of RSIL standards (prepared in the KOH/guaiacol eluted matrix) and their certified reference values. Error bars derived from measurement uncertainties are approximately equivalent to the size of the markers.

Appendix C: Deriving the N isotopic fractionation from isotopic exchange and the extended Leighton cycle

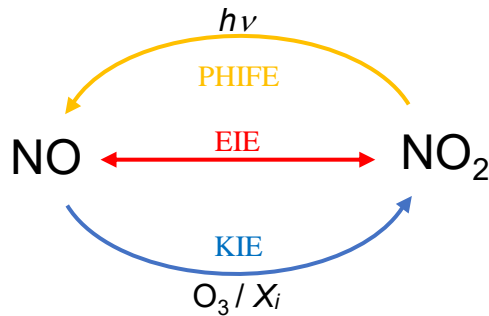


Figure C1. Sketch of the nitrogen fractionation processes between NO and NO₂. PHIFE for Photochemical Isotope Fractionation Effect, KIE for Kinetic Isotope Effect and EIE for Equilibrium Isotope Effect.

We follow the same approach as Li et al. (2020) but take into account all the oxidation pathways of NO into NO₂, not only via

535 O₃. The reactions considered in deriving the combined isotopic fractionation are the following:



with X_i = RO₂, BrO, ClO ...

545 Daytime N fractionation

During the day, NO₂ photolysis is the overwhelmingly dominant NO₂ sink and NO oxidation is the main NO₂ source. The assumption of steady-state on ¹⁵NO₂ for the extended Leighton cycle leads to

$$k_{\text{NO+NO}_2} [{}^{15}\text{NO}_2] [{}^{14}\text{NO}] + J_{\text{NO}_2} \alpha_{\text{PHIFE}} [{}^{15}\text{NO}_2] = \sum (k_{\text{NO+X}_i} \alpha_{\text{KIE}(\text{NO+X}_i)} [{}^{15}\text{NO}] [\text{X}_i]) + k_{\text{NO+NO}_2} \alpha_{\text{EIE}} [{}^{14}\text{NO}_2] [{}^{15}\text{NO}] \quad (\text{C1})$$

550 where $k_{\text{NO+NO}_2}$ is the rate constant for the nitrogen isotopic exchange between NO and NO₂, J_{NO_2} the NO₂ photolysis rate with α_{PHIFE} its isotopic fractionation factor, $\sum k_{\text{NO+X}_i} [\text{X}_i]$ the sum of all the NO oxidation pathways to NO₂, X_i the NO oxidant (i.e. O₃, RO₂, BrO, ClO...), and $k_{\text{NO+X}_i}$ the rate constant for the reaction of NO + X_i with $\alpha_{\text{KIE}(\text{NO+X}_i)}$ its isotopic fractionation factor. C1 can be rearranged to give

$$\frac{[{}^{15}\text{NO}_2]}{[{}^{15}\text{NO}]} = \frac{\sum (k_{\text{NO+X}_i} \alpha_{\text{KIE}(\text{NO+X}_i)} [\text{X}_i]) + k_{\text{NO+NO}_2} \alpha_{\text{EIE}} [{}^{14}\text{NO}_2]}{k_{\text{NO+NO}_2} [{}^{14}\text{NO}] + J_{\text{NO}_2} \alpha_{\text{PHIFE}}} \quad (\text{C2})$$

555 Meanwhile, ¹⁴NO₂ in steady-state leads to

$$\frac{[{}^{14}\text{NO}_2]}{[{}^{14}\text{NO}]} = \frac{\sum k_{\text{NO+X}_i} [\text{X}_i]}{J_{\text{NO}_2}} \quad (\text{C3})$$

We define A^*_{day} as the ratio of the ¹⁴NO₂ lifetime with respect to isotopic exchange with ¹⁴NO ($\tau_{\text{exchange-NO}_2}$) over the daytime ¹⁴NO₂ chemical lifetime ($\tau_{\text{chem-NO}_2}$) (Li et al., 2020):

$$A^*_{\text{day}} = \frac{\tau_{\text{exchange-NO}_2}}{\tau_{\text{chem-NO}_2}} = \frac{J_{\text{NO}_2}}{k_{\text{NO+NO}_2} [{}^{14}\text{NO}]} \quad (\text{C4})$$

560 Using C3, C4 becomes

$$A^*_{\text{day}} = \frac{\sum k_{\text{NO+X}_i} [\text{X}_i]}{k_{\text{NO+NO}_2} [{}^{14}\text{NO}_2]} \quad (\text{C5})$$

We also define $T_{\text{NO+X}_i}$ the relative importance of the oxidation pathway of NO into NO₂ via the oxidant X_i:

$$T_{\text{NO+X}_i} = \frac{k_{\text{NO+X}_i} [\text{X}_i]}{\sum k_{\text{NO+X}_i} [\text{X}_i]} \quad (\text{C6})$$

with necessarily $\sum T_{\text{NO+X}_i} = 1$.

565 Using the definitions C5 and C6, C2 becomes

$$\frac{[{}^{15}\text{NO}_2]}{[{}^{15}\text{NO}]} = \frac{A^*_{\text{day}} k_{\text{NO+NO}_2} [{}^{14}\text{NO}_2] \alpha_{\text{KIE}} + k_{\text{NO+NO}_2} \alpha_{\text{EIE}} [{}^{14}\text{NO}_2]}{k_{\text{NO+NO}_2} [{}^{14}\text{NO}] + A^*_{\text{day}} k_{\text{NO+NO}_2} [{}^{14}\text{NO}] \alpha_{\text{PHIFE}}} \quad (\text{C7})$$

with $\alpha_{\text{KIE}} = \sum T_{\text{NO+X}_i} + \alpha_{\text{KIE}(\text{NO+X}_i)}$

Using $R(^{15}\text{N}/^{14}\text{N}, \text{NO}) = R_{\text{NO}}(^{15}\text{N})/R_{\text{NO}}(^{14}\text{N}) = ^{15}R_{\text{NO}}$ (with $\delta^{15}\text{N}(\text{NO}) = ^{15}R_{\text{NO}}/^{15}R_{\text{standard}} - 1$) and $R(^{15}\text{N}/^{14}\text{N}, \text{NO}_2) = R_{\text{NO}_2}(^{15}\text{N})/R_{\text{NO}_2}(^{14}\text{N}) = ^{15}R_{\text{NO}_2}$ (with $\delta^{15}\text{N}(\text{NO}_2) = ^{15}R_{\text{NO}_2}/^{15}R_{\text{standard}} - 1$), C7 becomes

$$570 \quad \frac{^{15}R_{\text{NO}_2}}{^{15}R_{\text{NO}}} = \frac{[^{15}\text{NO}_2][^{14}\text{NO}]}{[^{15}\text{NO}][^{14}\text{NO}_2]} = \frac{A^*_{\text{day}} \alpha_{\text{KIE}} + \alpha_{\text{EIE}}}{1 + A^*_{\text{day}} \alpha_{\text{PHIFE}}} \quad (\text{C8})$$

$$\frac{^{15}R_{\text{NO}}}{^{15}R_{\text{NO}_2}} - 1 = \frac{A^*_{\text{day}}(\alpha_{\text{PHIFE}} - \alpha_{\text{KIE}}) - (\alpha_{\text{EIE}} - 1)}{A^*_{\text{day}} \alpha_{\text{KIE}} + \alpha_{\text{EIE}}} \quad (\text{C9})$$

As a result, the daytime isotopic shift of NO_2 relative to NO , defined as $\Delta(\text{NO}_2 - \text{NO}) = \delta^{15}\text{N}(\text{NO}_2) - \delta^{15}\text{N}(\text{NO})$, is given by

$$\Delta_{\text{day}}(\text{NO}_2 - \text{NO}) = \frac{A^*_{\text{day}}(\alpha_{\text{KIE}} - \alpha_{\text{PHIFE}}) + (\alpha_{\text{EIE}} - 1)}{A^*_{\text{day}} \alpha_{\text{KIE}} + \alpha_{\text{EIE}}} (1 + \delta^{15}\text{N}(\text{NO}_2)) \quad (\text{C10})$$

Using the isotopic balance $\delta^{15}\text{N}(\text{NO}_x) = f_{\text{NO}_2} \delta^{15}\text{N}(\text{NO}_2) + (1 - f_{\text{NO}_2}) \delta^{15}\text{N}(\text{NO})$ with $f_{\text{NO}_2} = [\text{NO}_2]/[\text{NO}_x]$ (Li et al. 2020), the 575 isotopic shift of NO_2 relative to NO_x , defined as $\Delta(\text{NO}_2 - \text{NO}_x) = \delta^{15}\text{N}(\text{NO}_2) - \delta^{15}\text{N}(\text{NO}_x)$, can be expressed by:

$$\Delta_{\text{day}}(\text{NO}_2 - \text{NO}_x) = \frac{A^*_{\text{day}}(\alpha_{\text{KIE}} - \alpha_{\text{PHIFE}}) + (\alpha_{\text{EIE}} - 1)}{A^*_{\text{day}} \alpha_{\text{KIE}} + \alpha_{\text{EIE}}} (1 + \delta^{15}\text{N}(\text{NO}_2))(1 - f_{\text{NO}_2}) \quad (\text{C11})$$

Since fractionation factors are close to unity and $1 + \delta^{15}\text{N}(\text{NO}_2) \approx 1$, C11 can be further simplified by keeping only the dominant terms (Li et al. 2020):

$$\Delta_{\text{day}}(\text{NO}_2 - \text{NO}_x) \approx \frac{\alpha_{\text{LCIE}}^* A^*_{\text{day}} + (\alpha_{\text{EIE}} - 1)}{A^*_{\text{day}} + 1} (1 - f_{\text{NO}_2}) \quad (\text{C12})$$

580 with $\alpha_{\text{LCIE}}^* = \alpha_{\text{KIE}} - \alpha_{\text{PHIFE}}$

Considering the localisation of our sampling site (urban mid-latitude area), only $\text{NO} + \text{RO}_2$ and $\text{NO} + \text{O}_3$ are thought to be significant as NO_2 formation pathways and hence α_{LCIE}^* becomes

$$\alpha_{\text{LCIE}}^* = T_{\text{NO}+\text{O}_3} \times \alpha_{\text{KIE}(\text{NO}+\text{O}_3)} + T_{\text{NO}+\text{RO}_2} \times \alpha_{\text{KIE}(\text{NO}+\text{RO}_2)} - \alpha_{\text{PHIFE}} \quad (\text{C13})$$

and C5 becomes

$$585 \quad A^*_{\text{day}} = \frac{k_{\text{NO}+\text{O}_3}[\text{O}_3] + k_{\text{NO}+\text{RO}_2}[\text{RO}_2]}{k_{\text{NO}+\text{NO}_2}[^{14}\text{NO}_2]} \quad (\text{C14})$$

Eq.4 and Eq.5 from section 4.1.2 can be combined to give

$$k_{\text{NO}+\text{O}_3}[\text{O}_3] + k_{\text{NO}+\text{RO}_2}[\text{RO}_2] = \frac{\Delta^{17}\text{O}_{\text{NO}+\text{O}_3}(\text{NO}_2)}{\Delta^{17}\text{O}_{\text{day}}(\text{NO}_2)} k_{\text{NO}+\text{O}_3}[\text{O}_3] \quad (\text{C15})$$

Using C15, C14 becomes

$$A^*_{\text{day}} = \frac{k_{\text{NO}+\text{O}_3}[\text{O}_3]}{k_{\text{NO}+\text{NO}_2}[\text{NO}_2]} \left(\frac{\Delta^{17}\text{O}_{\text{NO}+\text{O}_3(\text{NO}_2)}}{\Delta^{17}\text{O}_{\text{day}(\text{NO}_2)}} \right) \quad (\text{C16})$$

590 We consider several particular cases. The first case is when $\alpha_{\text{KIE}(\text{NO}+\text{O}_3)} \approx \alpha_{\text{KIE}(\text{NO}+\text{RO}_2)}$. Previous studies found that the NO + O₃ reaction falls within the family of “normal kinetic isotope fractionation” with the NO₂ produced being depleted in ¹⁵N (Walters and Michalski, 2016) compared to residual reactant NO. To our knowledge, no such experiment has been carried out for the NO + RO₂ reaction. Nonetheless, considering the very close, and both very low, activation energies for the reaction NO + O₃ and NO + RO₂, it is quite likely that the fractionation factors of these two reactions are similar. It follows that we 595 obtain the same expression for α_{LCIE}^* as for the α_{LCIE} given in Li et al. (2020):

$$\alpha_{\text{LCIE}}^* = \alpha_{\text{KIE}(\text{NO}+\text{O}_3)} - \alpha_{\text{PHIFE}} \quad (\text{C17})$$

And C12 becomes

$$\Delta_{\text{day}}(\text{NO}_2 - \text{NO}_x) = \frac{\alpha_{\text{LCIE}}^* A^*_{\text{day}} + (\alpha_{\text{EIE}} - 1)}{A^*_{\text{day}} + 1} (1 - f_{\text{NO}_2}) \quad (\text{C18})$$

C18 with A^*_{day} given by C16 is the expression that we use to analyse our daytime nitrogen isotopic measurements. Another 600 particular case considered by Li et al. (2020) is $k_{\text{NO}+\text{O}_3}[\text{O}_3] \gg k_{\text{NO}+\text{RO}_2}[\text{RO}_2]$; in that case, α_{LCIE}^* is still given by C12 but A^* is simplified:

$$A^*_{\text{day}} = \frac{k_{\text{NO}+\text{O}_3}[\text{O}_3]}{k_{\text{NO}+\text{NO}_2}[\text{NO}_2]} \quad (\text{C19})$$

C16 with A^*_{day} given by C19 and α_{LCIE}^* given by C17 is the same expression as Eq.8 in Li et al. (2020).

605 Nighttime N fractionation

An expression similar to C1 can be derived for nighttime conditions, when NO₂ photolysis is null and hence there is no recycling between NO and NO₂. In addition, the conversion of NO into NO₂ occurs only via reaction with O₃ because the mixing ratios of other NO oxidants are usually negligible at night. The main source of NO_x at night is the NO emissions. The assumption of steady-state on short time scales can only hold for ¹⁴NO and ¹⁵NO, not NO₂, leading to an equation equivalent 610 to C1:

$$k_{\text{NO}+\text{NO}_2}[\text{NO}_2][\text{NO}] + E(\text{NO})$$

$$= k_{\text{NO}+\text{O}_3} \alpha_{\text{KIE}} [{}^{15}\text{NO}] [\text{O}_3] + k_{\text{NO}+\text{NO}_2} \alpha_{\text{EIE}} [{}^{14}\text{NO}_2] [{}^{15}\text{NO}] \quad (\text{C20})$$

with $E({}^{15}\text{NO})$ being the ${}^{15}\text{NO}$ emission flux and α_{KIE} is the fractionation factor of $\text{NO} + \text{O}_3$. C20 can be rearranged to give

$$\frac{[{}^{15}\text{NO}_2]}{[{}^{15}\text{NO}]} = \frac{k_{\text{NO}+\text{O}_3} \alpha_{\text{KIE}} [\text{O}_3] + k_{\text{NO}+\text{NO}_2} \alpha_{\text{EIE}} [{}^{14}\text{NO}_2]}{k_{\text{NO}+\text{NO}_2} [{}^{14}\text{NO}] + E({}^{15}\text{NO}) / [{}^{15}\text{NO}_2]} \quad (\text{C21})$$

615 Meanwhile, the steady-state on ${}^{14}\text{NO}$ gives (nitrogen isotopic exchanges are neglected as NO emissions are largely dominated by ${}^{14}\text{NO}$):

$$E({}^{14}\text{NO}) = k_{\text{NO}+\text{O}_3} [{}^{14}\text{NO}] [\text{O}_3] \quad (\text{C22})$$

with $E({}^{14}\text{NO})$ being the ${}^{14}\text{NO}$ emission flux. For nighttime, we define A^*_{night} as the ratio of the ${}^{14}\text{NO}$ lifetime with respect to isotopic exchange with ${}^{14}\text{NO}_2$ ($\tau_{\text{exchange-NO}}$) over the nighttime ${}^{14}\text{NO}$ chemical lifetime ($\tau_{\text{chem-NO}}$):

$$620 \quad A^*_{\text{night}} = \frac{\tau_{\text{exchange-NO}}}{\tau_{\text{chem-NO}}} = \frac{k_{\text{NO}+\text{O}_3} [\text{O}_3]}{k_{\text{NO}+\text{NO}_2} [{}^{14}\text{NO}_2]} \quad (\text{C23})$$

Using C22, C23 gives

$$A^*_{\text{night}} = \frac{E({}^{14}\text{NO})}{k_{\text{NO}+\text{NO}_2} [{}^{14}\text{NO}] [{}^{14}\text{NO}_2]} \quad (\text{C24})$$

NO_x is overwhelmingly emitted in the form of NO. The isotopic signature of NO emissions can be characterised with ${}^{15}R_{\text{NO}_{\text{emis}}}$ and $\delta^{15}\text{N}(\text{NO}_{\text{emis}}) = {}^{15}R_{\text{NO}_{\text{emis}}} / {}^{15}R_{\text{standard}} - 1$. Using the definition of ${}^{15}R_{\text{NO}_{\text{emis}}}$, C23 and C24, C21 becomes

$$625 \quad \frac{[{}^{15}\text{NO}_2]}{[{}^{15}\text{NO}]} = \frac{A^*_{\text{night}} k_{\text{NO}+\text{NO}_2} [{}^{14}\text{NO}_2] \alpha_{\text{KIE}} + k_{\text{NO}+\text{NO}_2} \alpha_{\text{EIE}} [{}^{14}\text{NO}_2]}{k_{\text{NO}+\text{NO}_2} [{}^{14}\text{NO}] + ({}^{15}R_{\text{NO}_{\text{emis}}} E({}^{14}\text{NO})) / [{}^{15}\text{NO}_2]} \quad (\text{C25})$$

And then, using C24, C25 becomes

$$\frac{{}^{15}R_{\text{NO}_2}}{{}^{15}R_{\text{NO}}} = \frac{[{}^{15}\text{NO}_2] [{}^{14}\text{NO}]}{[{}^{15}\text{NO}] [{}^{14}\text{NO}_2]} = \frac{A^*_{\text{night}} \alpha_{\text{KIE}} + \alpha_{\text{EIE}}}{1 + A^*_{\text{night}} ({}^{15}R_{\text{NO}_{\text{emis}}} / {}^{15}R_{\text{NO}_2})} \quad (\text{C26})$$

$$\frac{{}^{15}R_{\text{NO}}}{{}^{15}R_{\text{NO}_2}} - 1 = \frac{A^*_{\text{night}} (({}^{15}R_{\text{NO}_{\text{emis}}} / {}^{15}R_{\text{NO}_2}) - \alpha_{\text{KIE}}) - (\alpha_{\text{EIE}} - 1)}{A^*_{\text{night}} \alpha_{\text{KIE}} + \alpha_{\text{EIE}}} \quad (\text{C27})$$

Following the approach used in the derivation of daytime isotopic shift, the nighttime isotopic shift of NO_2 relative to NO is 630 given by:

$$\Delta_{\text{night}}(\text{NO}_2 - \text{NO}) = \frac{A^*_{\text{night}} \left(\alpha_{\text{KIE}} - \left(\frac{\delta^{15}\text{NO}_{\text{emis}} / \delta^{15}\text{NO}_2}{1 + \delta^{15}\text{N}(\text{NO}_2)} \right) \right) + (\alpha_{\text{EIE}} - 1)}{A^*_{\text{night}} \alpha_{\text{KIE}} + \alpha_{\text{EIE}}} (1 + \delta^{15}\text{N}(\text{NO}_2)) \quad (\text{C28})$$

Using the isotopic balance $\delta^{15}\text{N}(\text{NO}_x) = f_{\text{NO}_2} \delta^{15}\text{N}(\text{NO}_2) + (1 - f_{\text{NO}_2}) \delta^{15}\text{N}(\text{NO})$, the nighttime isotopic shift of NO_2 relative to NO_x , can be expressed by:

$$\Delta_{\text{night}}(\text{NO}_2 - \text{NO}_x) = \frac{A^*_{\text{night}} \left(\alpha_{\text{KIE}} - \left(\frac{1 + \delta^{15}\text{N}(\text{NO}_{\text{emis}})}{1 + \delta^{15}\text{N}(\text{NO}_2)} \right) \right) + (\alpha_{\text{EIE}} - 1)}{A^*_{\text{night}} \alpha_{\text{KIE}} + \alpha_{\text{EIE}}} (1 + \delta^{15}\text{N}(\text{NO}_2))(1 - f_{\text{NO}_2}) \quad (\text{C29})$$

635 where $\delta^{15}\text{N}(\text{NO}_{\text{emis}})$ is the nitrogen isotopic composition of NO emissions.

Keeping the dominant terms, C29 can be further simplified following the daytime derivation:

$$\Delta_{\text{night}}(\text{NO}_2 - \text{NO}_x) \approx \frac{A^*_{\text{night}} \left(\alpha_{\text{KIE}} - \left(\frac{1 + \delta^{15}\text{N}(\text{NO}_{\text{emis}})}{1 + \delta^{15}\text{N}(\text{NO}_2)} \right) \right) + (\alpha_{\text{EIE}} - 1)}{A^*_{\text{night}} + 1} (1 - f_{\text{NO}_2}) \quad (\text{C30})$$

We consider two particular cases. When $A^*_{\text{night}} \ll 1$ ($k_{\text{NO}+\text{NO}_2}[\text{NO}_2] \gg k_{\text{NO}+\text{O}_3}[\text{O}_3]$) i.e isotopic exchange much faster than NO oxidation, C28 becomes

$$640 \quad \Delta_{\text{night}}(\text{NO}_2 - \text{NO}) = \frac{(\alpha_{\text{EIE}} - 1)}{\alpha_{\text{EIE}}} (1 + \delta^{15}\text{N}(\text{NO}_2)) \quad (\text{C31})$$

Keeping the dominant terms, C31 can be simplified

$$\Delta_{\text{night}}(\text{NO}_2 - \text{NO}) \approx (\alpha_{\text{EIE}} - 1) \quad (\text{C32})$$

As expected, the nighttime isotopic shift of NO_2 relative to NO depends only on the isotopic exchange fractionation in that case. In the same way, C29 becomes

$$645 \quad \Delta_{\text{night}}(\text{NO}_2 - \text{NO}_x) = \frac{(\alpha_{\text{EIE}} - 1)}{\alpha_{\text{EIE}}} (1 + \delta^{15}\text{N}(\text{NO}_2))(1 - f_{\text{NO}_2}) \quad (\text{C33})$$

Keeping the dominant terms, C33 can be simplified

$$\Delta_{\text{night}}(\text{NO}_2 - \text{NO}_x) \approx \frac{(\alpha_{\text{EIE}} - 1)}{\alpha_{\text{EIE}}} (1 - f_{\text{NO}_2}) \quad (\text{C34})$$

When $A^*_{\text{night}} \gg 1$ ($k_{\text{NO}+\text{NO}_2}[\text{NO}_2] \ll k_{\text{NO}+\text{O}_3}[\text{O}_3]$) i.e NO oxidation much faster than isotopic exchange, C28 yields

$$\Delta_{\text{night}}(\text{NO}_2 - \text{NO}) = 1 + \delta^{15}\text{N}(\text{NO}_2) - \left(\frac{1 + \delta^{15}\text{N}(\text{NO}_{\text{emis}})}{\alpha_{\text{KIE}}} \right) \quad (\text{C35})$$

650 leading to

$$1 + \delta^{15}\text{N}(\text{NO}) = \left(\frac{1 + \delta^{15}\text{N}(\text{NO}_{\text{emis}})}{\alpha_{\text{KIE}}} \right) \quad (\text{C36})$$

$$^{15}R_{\text{NO}} = \frac{^{15}R_{\text{NO}_{\text{emis}}}}{\alpha_{\text{KIE}}} \quad (\text{C37})$$

As expected, the nighttime isotopic shift of NO relative to NO emissions depends only on the isotopic fractionation factor of the $\text{NO} + \text{O}_3$ reaction in that case. It is possible to estimate the nighttime isotopic shift of NO_2 relative to NO or NO_x on long 655 timescales by assuming crudely that $^{14}\text{NO}_2$ is in steady-state:

$$k_{\text{loss-NO}_2}[^{14}\text{NO}_2] = k_{\text{NO+O}_3}[^{14}\text{NO}][\text{O}_3] \quad (\text{C38})$$

with $k_{\text{loss-NO}_2}$ representing the equivalent of a first-order rate constant. If the $^{14}\text{NO}_2$ loss is a second-order reaction such as $\text{NO}_2 + \text{O}_3$ loss, $k_{\text{loss-NO}_2} = k_{\text{NO}_2+\text{O}_3}[\text{O}_3]$. In the same way, assuming that the NO_2 oxidation into nitrate via O_3 is not fractionating, $^{15}\text{NO}_2$ in steady-state gives:

$$660 \quad k_{\text{loss-NO}_2}[^{15}\text{NO}_2] = k_{\text{NO+O}_3}\alpha_{\text{KIE}}[^{15}\text{NO}][\text{O}_3] \quad (\text{C39})$$

Using C38, C39 becomes

$$^{15}R_{\text{NO}_2} = \alpha_{\text{KIE}}^{15}R_{\text{NO}} \quad (\text{C40})$$

Using C37, C40 becomes

$$^{15}R_{\text{NO}_2} = ^{15}R_{\text{NO,emis}} \quad (\text{C41})$$

665 Or

$$\delta^{15}\text{N}(\text{NO}_2) = \delta^{15}\text{N}(\text{NO}_{\text{emis}}) \quad (\text{C42})$$

Under those conditions (negligible isotopic exchange), a measurement of $\delta^{15}\text{N}(\text{NO}_2)$ is a measurement of $\delta^{15}\text{N}(\text{NO}_{\text{emis}})$, preferably towards the end of the night in order for $^{14}\text{NO}_2$ to move towards steady-state.

In the text, $^{14}\text{NO}_2$ and ^{14}NO are referred as NO_2 and NO for convenience.

Appendix D: kinetic data used

reaction number	Reactions	Rate constants /cm ³ mol ⁻¹ s ⁻¹	References
R3	$\text{NO} + \text{O}_3 \rightarrow \text{NO}_2 + \text{O}_2$	$k_{\text{NO}+\text{O}_3} = 1.4 \times 10^{-12} \exp(-1310(\text{K})/\text{T})$	Atkinson et al. (2004)
R4	$\text{NO} + \text{RO}_2 \rightarrow \text{NO}_2 + \text{RO}$	$k_{\text{NO}+\text{RO}_2} = 2.3 \times 10^{-12} \exp(360(\text{K})/\text{T})$	Atkinson et al. (2006)
R6	$\text{NO}_2 + \text{O}_3 \xrightarrow{\text{M}} \text{NO}_3 + \text{O}_2$	$k_{\text{NO}_2+\text{O}_3} = 1.4 \times 10^{-13} \exp(-2470(\text{K})/\text{T})$	Atkinson et al. (2004)
CR1	$^{15}\text{NO}_2 + ^{14}\text{NO} \rightarrow ^{14}\text{NO}_2 + ^{15}\text{NO}$	$k_{\text{NO}+\text{NO}_2} = 8.14 \times 10^{-14}$	Sharma et al. (1970)

Table D1. Rate constants used for calculations

675 *Author contribution.* Sampling and analysis protocol were developed by SA under the supervision of JS. NC and AB contributed with technical and knowledge support to SA for isotopic mass spectrometry and more general atmospheric measurements. SB and JS, supervisors of SA PhD Thesis, helped SA in interpreting the results and writing the manuscript.

Competing interests. The authors have no conflict of interests to report.

Acknowledgements. This work benefited from the IGE infrastructures and laboratory platforms. This is the publication number 2 of the PANDA platform on which isotope analyses were performed, partially supported by the ANR project ANR-15-IDEX-02 and Labex OSUG@2020, Investissements d'avenir – ANR10 LABX56. The authors acknowledge the support of the ALPACA program (Alaskan Layered Pollution and Chemical Analysis) funded by two French research organisms: the French polar institute (IPEV, Institut polaire français Paul-Emile Victor) and INSU-CNRS (National Institute of Sciences of the Universe) via its national LEFE program (Les Enveloppes Fluides et l'Environnement). Finally, the authors thank E. Gauthier, S. Darfeuil and P. Akers for help with laboratory work and more general scientific discussions.

References

690 Alexander, B., Hastings, M. G., Allman, D. J., Dachs, J., Thornton, J. A., and Kunasek, S. A.: Quantifying atmospheric nitrate formation pathways based on a global model of the oxygen isotopic composition ($\Delta^{17}\text{O}$) of atmospheric nitrate, *Atmospheric Chem. Phys.*, 9, 5043–5056, <https://doi.org/10.5194/acp-9-5043-2009>, 2009.

Alexander, B., Sherwen, T., Holmes, C. D., Fisher, J. A., Chen, Q., Evans, M. J., and Kasibhatla, P.: Global inorganic nitrate production mechanisms: comparison of a global model with nitrate isotope observations, *Atmospheric Chem. Phys.*, 20, 3859–3877, <https://doi.org/10.5194/acp-20-3859-2020>, 2020.

695 Assonov, S. S. and Brenninkmeijer, C. a. M.: Reporting small $\Delta^{17}\text{O}$ values: existing definitions and concepts, *Rapid Commun. Mass Spectrom.*, 19, 627–636, <https://doi.org/10.1002/rcm.1833>, 2005.

Atkinson, R., Baulch, D. L., Cox, R. A., Hampson, R. F., Kerr, J. A., Rossi, M. J., and Troe, J.: Evaluated Kinetic, Photochemical and Heterogeneous Data for Atmospheric Chemistry: Supplement V. IUPAC Subcommittee on Gas Kinetic Data Evaluation for Atmospheric Chemistry, *J. Phys. Chem. Ref. Data*, 26, 521–1011, <https://doi.org/10.1063/1.556011>, 1997.

700 Atkinson, R., Baulch, D. L., Cox, R. A., Crowley, J. N., Hampson, R. F., Hynes, R. G., Jenkin, M. E., Rossi, M. J., and Troe, J.: Evaluated kinetic and photochemical data for atmospheric chemistry: Volume I - gas phase reactions of O_x , HO_x , NO_x and SO_x species, *Atmospheric Chem. Phys.*, 4, 1461–1738, <https://doi.org/10.5194/acp-4-1461-2004>, 2004.

Atkinson, R., Baulch, D. L., Cox, R. A., Crowley, J. N., Hampson, R. F., Hynes, R. G., Jenkin, M. E., Rossi, M. J., Troe, J., and IUPAC Subcommittee: Evaluated kinetic and photochemical data for atmospheric chemistry: Volume II - gas phase reactions of organic species, *Atmospheric Chem. Phys.*, 6, 3625–4055, <https://doi.org/10.5194/acp-6-3625-2006>, 2006.

705 Atmo-Auvergne-Rhônes-Alpes: Bilan Qualité de l'Air 2018 – Isère, <https://doi.org/www.atmo-auvergnehonealpes.fr>, 2018.

Barkan, E. and Luz, B.: High-precision measurements of $^{17}\text{O}/^{16}\text{O}$ and $^{18}\text{O}/^{16}\text{O}$ of O_2 and O_2/Ar ratio in air, *Rapid Commun. Mass Spectrom.*, 17, 2809–2814, <https://doi.org/10.1002/rcm.1267>, 2003.

710 Böhlke, J. K., Smith, R. L., and Hannon, J. E.: Isotopic Analysis of N and O in Nitrite and Nitrate by Sequential Selective Bacterial Reduction to N_2O , *Anal. Chem.*, 79, 5888–5895, <https://doi.org/10.1021/ac070176k>, 2007.

Brand, W. A.: High Precision Isotope Ratio Monitoring Techniques in Mass Spectrometry, *J. Mass Spectrom.*, 31, 225–235, [https://doi.org/10.1002/\(SICI\)1096-9888\(199603\)31:3<225::AID-JMS319>3.0.CO;2-L](https://doi.org/10.1002/(SICI)1096-9888(199603)31:3<225::AID-JMS319>3.0.CO;2-L), 1996.

Brown, S. S.: Variability in Nocturnal Nitrogen Oxide Processing and Its Role in Regional Air Quality, *Science*, 311, 67–70, <https://doi.org/10.1126/science.1120120>, 2006.

715 Buttini, P., Di Palo, V., and Possanzini, M.: Coupling of denuder and ion chromatographic techniques for NO_2 trace level determination in air, *Sci. Total Environ.*, 61, 59–72, [https://doi.org/10.1016/0048-9697\(87\)90356-1](https://doi.org/10.1016/0048-9697(87)90356-1), 1987.

Casciotti, K. L., Sigman, D. M., Hastings, M. G., Böhlke, J. K., and Hilkert, A.: Measurement of the oxygen isotopic composition of nitrate in seawater and freshwater using the denitrifier method, *Anal. Chem.*, 74, 4905–4912, <https://doi.org/10.1021/ac020113w>, 2002.

720 Crutzen, P. J.: My life with O_3 , NO_x and other YZO_x compounds (Nobel lecture), *Angew. Chem. Int Ed Engl.*, 35, 1759–1776, 1996.

Dahal, B. and Hastings, M. G.: Technical considerations for the use of passive samplers to quantify the isotopic composition of NO_x and NO_2 using the denitrifier method, *Atmos. Environ.*, 143, 60–66, <https://doi.org/10.1016/j.atmosenv.2016.08.006>, 2016.

725 Dallmann, T. R., Kirchstetter, T. W., DeMartini, S. J., and Harley, R. A.: Quantifying On-Road Emissions from Gasoline-Powered Motor Vehicles: Accounting for the Presence of Medium- and Heavy-Duty Diesel Trucks, *Environ. Sci. Technol.*, 47, 13873–13881, <https://doi.org/10.1021/es402875u>, 2013.

Davidson, E. A. and Kingerlee, W.: A global inventory of nitric oxide emissions from soils, *Nutr. Cycl. Agroecosystems*, 48, 37–50, <https://doi.org/10.1023/A:1009738715891>, 1997.

730 Dennison, P., Charoensiri, K., Roberts, D., Peterson, S., and Green, R.: Wildfire temperature and land cover modeling using hyperspectral data, *Remote Sens. Environ.*, 100, 212–222, <https://doi.org/10.1016/j.rse.2005.10.007>, 2006.

Fan, M.-Y., Zhang, Y.-L., Lin, Y.-C., Chang, Y.-H., Cao, F., Zhang, W.-Q., Hu, Y.-B., Bao, M.-Y., Liu, X.-Y., Zhai, X.-Y., Lin, X., Zhao, Z.-Y., and Song, W.-H.: Isotope-based source apportionment of nitrogen-containing aerosols: A case study in an industrial city in China, *Atmos. Environ.*, 212, 96–105, <https://doi.org/10.1016/j.atmosenv.2019.05.020>, 2019.

735 Felix, J. D. and Elliott, E. M.: Isotopic composition of passively collected nitrogen dioxide emissions: Vehicle, soil and livestock source signatures, *Atmos. Environ.*, 92, 359–366, <https://doi.org/10.1016/j.atmosenv.2014.04.005>, 2014.

Finlayson-Pitts, B. J. and Pitts, J. N.: Chemistry of the Upper and Lower Atmosphere, Elsevier, <https://doi.org/10.1016/B978-012257060-5/50003-4>, 2000.

740 Freyer, H. D., Kley, D., Volz-Thomas, A., and Kobel, K.: On the interaction of isotopic exchange processes with photochemical reactions in atmospheric oxides of nitrogen, *J. Geophys. Res. Atmospheres*, 98, 14791–14796, <https://doi.org/10.1029/93JD00874>, 1993.

Fuchs, H., Holland, F., and Hofzumahaus, A.: Measurement of tropospheric RO₂ and HO₂ radicals by a laser-induced fluorescence instrument, *Rev. Sci. Instrum.*, 79, 084104, <https://doi.org/10.1063/1.2968712>, 2008.

745 Galloway, J. N., Dentener, F. J., Capone, D. G., Boyer, E. W., Howarth, R. W., Seitzinger, S. P., Asner, G. P., Cleveland, C. C., Green, P. A., Holland, E. A., Karl, D. M., Michaels, A. F., Porter, J. H., Townsend, A. R., and Vöosmarty, C. J.: Nitrogen Cycles: Past, Present, and Future, *Biogeochemistry*, 70, 153–226, <https://doi.org/10.1007/s10533-004-0370-0>, 2004.

Geng, F., Tie, X., Xu, J., Zhou, G., Peng, L., Gao, W., Tang, X., and Zhao, C.: Characterizations of ozone, NO_x and VOCs measured in Shanghai, China, *Atmos. Environ.*, 42, 6873–6883, <https://doi.org/10.1016/j.atmosenv.2008.05.045>, 2008.

750 Harris, G. W., Carter, W. P. L., Winer, A. M., Pitts, J. N., Platt, Ulrich., and Perner, Dieter.: Observations of nitrous acid in the Los Angeles atmosphere and implications for predictions of ozone-precursor relationships, *Environ. Sci. Technol.*, 16, 414–419, <https://doi.org/10.1021/es00101a009>, 1982.

Holland, E. A., Dentener, F. J., Braswell, B. H., and Sulzman, J. M.: Contemporary and pre-industrial global reactive nitrogen budgets, *Biogeochemistry*, 46, 7–43, <https://doi.org/10.1023/A:1006148011944>, 1999.

755 Huang, R.-J., Yang, L., Cao, J., Wang, Q., Tie, X., Ho, K.-F., Shen, Z., Zhang, R., Li, G., Zhu, C., Zhang, N., Dai, W., Zhou, J., Liu, S., Chen, Y., Chen, J., and O'Dowd, C. D.: Concentration and sources of atmospheric nitrous acid (HONO) at an urban site in Western China, *Sci. Total Environ.*, 593–594, 165–172, <https://doi.org/10.1016/j.scitotenv.2017.02.166>, 2017.

Inger, R., Ruxton, G. D., Newton, J., Colhoun, K., Robinson, J. A., Jackson, A. L., and Bearhop, S.: Temporal and intrapopulation variation in prey choice of wintering geese determined by stable isotope analysis, *J. Anim. Ecol.*, 75, 1190–1200, <https://doi.org/10.1111/j.1365-2656.2006.01142.x>, 2006.

760 Jacob, D. J.: Introduction to Atmospheric Chemistry, Princeton Univ. Press, 1999.

Jin, S. and Demerjian, K.: A photochemical box model for urban air quality study, *Atmospheric Environ. Part B Urban Atmosphere*, 27, 371–387, [https://doi.org/10.1016/0957-1272\(93\)90015-X](https://doi.org/10.1016/0957-1272(93)90015-X), 1993.

Jin, Z., Qian, L., Shi, Y., Fu, G., Li, G., and Li, F.: Quantifying major NO_x sources of aerosol nitrate in Hangzhou, China, by using stable isotopes and a Bayesian isotope mixing model, *Atmos. Environ.*, 244, 117979, <https://doi.org/10.1016/j.atmosenv.2020.117979>, 2021.

Johnston, J. C. and Thiemens, M. H.: The isotopic composition of tropospheric ozone in three environments, *J. Geophys. Res. Atmospheres*, 102, 25395–25404, 1997.

Kaiser, J., Röckmann, T., and Brenninkmeijer, C. A. M.: Contribution of mass-dependent fractionation to the oxygen isotope anomaly of atmospheric nitrous oxide, *J. Geophys. Res. Atmospheres*, 109, D03305, <https://doi.org/10.1029/2003JD004088>, 2004.

Kaiser, J., Hastings, M. G., Houlton, B. Z., Röckmann, T., and Sigman, D. M.: Triple oxygen isotope analysis of nitrate using the denitrifier method and thermal decomposition of N₂O, *Anal. Chem.*, 79, 599–607, <https://doi.org/10.1021/ac061022s>, 2007.

Kaye, J. A.: Mechanisms and observations for isotope fractionation of molecular species in planetary atmospheres, *Rev. Geophys.*, 25, 1609–1658, <https://doi.org/10.1029/RG025i008p01609>, 1987.

Klein, A., Ravetta, F., Thomas, J. L., Ancellet, G., Augustin, P., Wilson, R., Dieudonné, E., Fourmentin, M., Delbarre, H., and Pelon, J.: Influence of vertical mixing and nighttime transport on surface ozone variability in the morning in Paris and the surrounding region, *Atmos. Environ.*, 197, 92–102, <https://doi.org/10.1016/j.atmosenv.2018.10.009>, 2019.

Kleinman, L. I., Daum, P. H., Lee, Y.-N., Nunnermacker, L. J., Springston, S. R., Weinstein-Lloyd, J., and Rudolph, J.: Ozone production efficiency in an urban area, *J. Geophys. Res. Atmospheres*, 107, 4733, <https://doi.org/10.1029/2002JD002529>, 2002.

Kobayashi, K., Fukushima, K., Onishi, Y., Nishina, K., Makabe, A., Yano, M., Wankel, S. D., Koba, K., and Okabe, S.: Influence of $\delta^{18}\text{O}$ of water on measurements of $\delta^{18}\text{O}$ of nitrite and nitrate, *Rapid Commun. Mass Spectrom.*, n/a, <https://doi.org/10.1002/rcm.8979>, 2020.

Krankowsky, D., Bartecki, F., Klees, G. G., Mauersberger, K., Schellenbach, K., and Stehr, J.: Measurement of heavy isotope enrichment in tropospheric ozone, *Geophys. Res. Lett.*, 22, 1713–1716, 1995.

Largeron, Y. and Staquet, C.: Persistent inversion dynamics and wintertime PM₁₀ air pollution in Alpine valleys, *Atmos. Environ.*, 135, 92–108, <https://doi.org/10.1016/j.atmosenv.2016.03.045>, 2016.

Leighton, P. A.: Photochemistry of Air Pollution., Acad. Press, 66, 279–279, <https://doi.org/10.1002/bbpc.19620660323>, 1961.

Li, D. and Wang, X.: Nitrogen isotopic signature of soil-released nitric oxide (NO) after fertilizer application, *Atmos. Environ.*, 42, 4747–4754, <https://doi.org/10.1016/j.atmosenv.2008.01.042>, 2008.

Li, J., Zhang, X., Orlando, J., Tyndall, G., and Michalski, G.: Quantifying the nitrogen isotope effects during photochemical equilibrium between NO and NO₂: implications for $\delta^{15}\text{N}$ in tropospheric reactive nitrogen, *Atmospheric Chem. Phys.*, 20, 9805–9819, <https://doi.org/10.5194/acp-20-9805-2020>, 2020.

Li, W., Ni, B. L., Jin, D. Q., and Zhang, Q. G.: Measurement of the absolute abundance of Oxygen-17 in SMOW, *Kexue Tongboa Chin. Sci. Bull.*, 33 (19), 1610–1613, <https://doi.org/10.1360/sb1988-33-19-1610>, 1988.

Liao, H. and Seinfeld, J. H.: Global impacts of gas-phase chemistry-aerosol interactions on direct radiative forcing by anthropogenic aerosols and ozone, *J. Geophys. Res. Atmospheres*, 110, <https://doi.org/10.1029/2005JD005907>, 2005.

Lyons, J. R.: Transfer of mass-independent fractionation in ozone to other oxygen-containing radicals in the atmosphere, *Geophys. Res. Lett.*, 28, 3231–3234, <https://doi.org/10.1029/2000GL012791>, 2001.

Mariotti, A.: Natural ^{15}N abundance measurements and atmospheric nitrogen standard calibration, *Nature*, 311, 251, <https://doi.org/10.1038/311251a0>, 1984.

Mayer, H.: Air pollution in cities, *Atmos. Environ.*, 33, 4029–4037, [https://doi.org/10.1016/S1352-2310\(99\)00144-2](https://doi.org/10.1016/S1352-2310(99)00144-2), 1999.

McIlvin, M. R. and Altabet, M. A.: Chemical Conversion of Nitrate and Nitrite to Nitrous Oxide for Nitrogen and Oxygen Isotopic Analysis in Freshwater and Seawater, *Anal. Chem.*, 77, 5589–5595, <https://doi.org/10.1021/ac050528s>, 2005.

805 Michalski, G., Scott, Z., Kabiling, M., and Thiemens, M. H.: First measurements and modeling of $\Delta^{17}\text{O}$ in atmospheric nitrate., *Geophys. Res. Lett.*, 30, <https://doi.org/10.1029/2003GL017015>, 2003.

Michalski, G., Bhattacharya, S. K., and Girsch, G.: NO_x cycle and the tropospheric ozone isotope anomaly: an experimental investigation, *Atmospheric Chem. Phys.*, 14, 4935–4953, <https://doi.org/10.5194/acp-14-4935-2014>, 2014.

810 Michoud, V., Colomb, A., Borbon, A., Miet, K., Beekmann, M., Camredon, M., Aumont, B., Perrier, S., Zapf, P., Siour, G., Ait-Helal, W., Afif, C., Kukui, A., Furger, M., Dupont, J. C., Haeffelin, M., and Doussin, J. F.: Study of the unknown HONO daytime source at a European suburban site during the MEGAPOLI summer and winter field campaigns, *Atmospheric Chem. Phys.*, 14, 2805–2822, <https://doi.org/10.5194/acp-14-2805-2014>, 2014.

815 Miller, D. J., Wojtal, P. K., Clark, S. C., and Hastings, M. G.: Vehicle NO_x emission plume isotopic signatures: Spatial variability across the eastern United States, *J. Geophys. Res. Atmospheres*, 122, 4698–4717, <https://doi.org/10.1002/2016JD025877>, 2017.

Miller, D. J., Chai, J., Guo, F., Dell, C. J., Karsten, H., and Hastings, M. G.: Isotopic Composition of In Situ Soil NO_x Emissions in Manure-Fertilized Cropland, *Geophys. Res. Lett.*, 45, 12,058–12,066, <https://doi.org/10.1029/2018GL079619>, 2018.

820 Monks, P. S.: Gas-phase radical chemistry in the troposphere, *Chem. Soc. Rev.*, 34, 376–395, <https://doi.org/10.1039/B307982C>, 2005.

Morin, S.: Analyse de la composition isotopique de l'ion nitrate dans la basse atmosphère polaire et marine. *Science de la Terre*, PhD-Thesis, Université Paris-Est, France, 281 pp., 2008.

825 Morin, S., Savarino, J., Bekki, S., Gong, S., and Bottenheim, J. W.: Signature of Arctic surface ozone depletion events in the isotope anomaly ($\Delta^{17}\text{O}$) of atmospheric nitrate, *Atmos. Chem. Phys.*, 7, 1451–1469, <https://doi.org/10.5194/acp-7-1451-2007>, 2007.

Morin, S., Sander, R., and Savarino, J.: Simulation of the diurnal variations of the oxygen isotope anomaly ($\Delta^{17}\text{O}$) of reactive atmospheric species, *Atmospheric Chem. Phys.*, 11, 3653–3671, <https://doi.org/10.5194/acp-11-3653-2011>, 2011.

Nash, T.: An efficient absorbing reagent for nitrogen dioxide, *Atmospheric Environ.* 1967, 4, 661–665, [https://doi.org/10.1016/0004-6981\(70\)90039-9](https://doi.org/10.1016/0004-6981(70)90039-9), 1970.

830 Parnell, A. C., Inger, R., Bearhop, S., and Jackson, A. L.: Source Partitioning Using Stable Isotopes: Coping with Too Much Variation, *PLOS ONE*, 5, e9672, <https://doi.org/10.1371/journal.pone.0009672>, 2010.

Prinn, R. G.: The Cleasing Capacity of the Atmosphere, *Annu. Rev. Environ. Resour.*, 28, 29–57, <https://doi.org/10.1146/annurev.energy.28.011503.163425>, 2003.

835 Röckmann, T., Kaiser, J., Crowley, J. N., Brenninkmeijer, C. A. M., and Crutzen, P. J.: The origin of the anomalous or “mass-independent” oxygen isotope fractionation in tropospheric N_2O , *Geophys. Res. Lett.*, 28, 503–506, <https://doi.org/10.1029/2000GL012295>, 2001.

Røyset, O.: Comparison of passive and active sampling methods for the determination of nitrogen dioxide in urban air, *Fresenius J. Anal. Chem.*, 360, 69–73, <https://doi.org/10.1007/s002160050644>, 1998.

840 Samelius, G., Alisauskas, R. T., Hobson, K. A., and Larivière, S.: Prolonging the arctic pulse: long-term exploitation of cached eggs by arctic foxes when lemmings are scarce, *J. Anim. Ecol.*, 76, 873–880, <https://doi.org/10.1111/j.1365-2656.2007.01278.x>, 2007.

Savarino, J., Bhattacharya, S. K., Morin, S., Baroni, M., and Doussin, J.-F.: The $\text{NO}+\text{O}_3$ reaction: A triple oxygen isotope perspective on the reaction dynamics and atmospheric implications for the transfer of the ozone isotope anomaly, *J. Chem. Phys.*, 128, 194303, <https://doi.org/10.1063/1.2917581>, 2008.

845 Seinfeld, J. H. and Pandis, S. N.: *Atmospheric chemistry and physics: from air pollution to climate change*, 2nd ed., Wiley, Hoboken, NJ, 1203 pp., 2006.

Sharma, H. D., Jervis, R. E., and Wong, K. Y.: Isotopic exchange reactions in nitrogen oxides, *J. Phys. Chem.*, 74, 923–933, <https://doi.org/10.1021/j100699a044>, 1970.

850 Tan, Z., Fuchs, H., Lu, K., Hofzumahaus, A., Bohn, B., Broch, S., Dong, H., Gomm, S., Häseler, R., He, L., Holland, F., Li, X., Liu, Y., Lu, S., Rohrer, F., Shao, M., Wang, B., Wang, M., Wu, Y., Zeng, L., Zhang, Y., Wahner, A., and Zhang, Y.: Radical chemistry at a rural site (Wangdu) in the North China Plain: observation and model calculations of OH , HO_2 and RO_2 radicals, *Atmospheric Chem. Phys.*, 17, 663–690, <https://doi.org/10.5194/acp-17-663-2017>, 2017.

Thiemens, M. H.: Mass-Independent Isotope Effects in Planetary Atmospheres and the Early Solar System, *Science*, 283, 341–345, <https://doi.org/10.1126/science.283.5400.341>, 1999.

855 Thiemens, M. H. and Heidenreich, J. E.: The Mass-Independent Fractionation of Oxygen: A Novel Isotope Effect and Its Possible Cosmochemical Implications, *Science*, 219, 1073–1075, <https://doi.org/10.1126/science.219.4588.1073>, 1983.

Tie, X., Madronich, S., Li, G., Ying, Z., Zhang, R., Garcia, A. R., Lee-Taylor, J., and Liu, Y.: Characterizations of chemical oxidants in Mexico City: A regional chemical dynamical model (WRF-Chem) study, *Atmos. Environ.*, 41, 1989–2008, <https://doi.org/10.1016/j.atmosenv.2006.10.053>, 2007.

860 Topin, C., Mouthuy, L., Colomer, C., and Chauvin, P.: Rapport de l’Evaluaton Environnementale Stratégique du PCAET 2020-2030 de Grenoble Alpes Métropole, 2019.

Urey, H. C.: The thermodynamic properties of isotopic substances, *J. Chem. Soc.*, 562–581, <https://doi.org/10.1039/JR9470000562>, 1947.

Velasco, E., Márquez, C., Bueno, E., Bernabé, R. M., Sánchez, A., Fentanes, O., Wöhrnschimmel, H., Cárdenas, B., Kamilla, A., Wakamatsu, S., and Molina, L. T.: Vertical distribution of ozone and VOCs in the low boundary layer of Mexico City, *Atmospheric Chem. Phys.*, 8, 3061–3079, <https://doi.org/10.5194/acp-8-3061-2008>, 2008.

Vicars, W. C. and Savarino, J.: Quantitative constraints on the ^{17}O -excess ($\Delta^{17}\text{O}$) signature of surface ozone: Ambient measurements from 50°N to 50°S using the nitrite-coated filter technique, *Geochim. Cosmochim. Acta*, 135, 270–287, <https://doi.org/10.1016/j.gca.2014.03.023>, 2014.

870 Villena, G., Kleffmann, J., Kurtenbach, R., Wiesen, P., Lissi, E., Rubio, M. A., Croxatto, G., and Rappenglück, B.: Vertical gradients of HONO, NO_x and O₃ in Santiago de Chile, *Atmos. Environ.*, 45, 3867–3873, <https://doi.org/10.1016/j.atmosenv.2011.01.073>, 2011.

Walters, W. W. and Michalski, G.: Ab initio study of nitrogen and position-specific oxygen kinetic isotope effects in the NO + O₃ reaction, *J. Chem. Phys.*, 145, 224311, <https://doi.org/10.1063/1.4968562>, 2016.

875 Walters, W. W., Tharp, B. D., Fang, H., Kozak, B. J., and Michalski, G.: Nitrogen isotope composition of thermally produced NO_x from various fossil-fuel combustion sources, *Environ. Sci. Technol.*, 49, 11363–11371, <https://doi.org/10.1021/acs.est.5b02769>, 2015.

Walters, W. W., Fang, H., and Michalski, G.: Summertime diurnal variations in the isotopic composition of atmospheric nitrogen dioxide at a small midwestern United States city, *Atmos. Environ.*, 179, 1–11, 880 <https://doi.org/10.1016/j.atmosenv.2018.01.047>, 2018.

Williams, E. L. and Grosjean, D.: Removal of atmospheric oxidants with annular denuders, *Environ. Sci. Technol.*, 24, 811–814, <https://doi.org/10.1021/es00076a002>, 1990.

885 Young, G. L.: NO_x formation in rotary kilns producing cement clinker applicable NO_x control techniques and cost effectiveness of these control techniques, in: Conference record- IEEE Cement Industry Technical Conference, IEEE Piscataway NJ U, 239–254, <https://doi.org/10.1109/CITCON.2002.1006510>, 2002.

Yu, Z. and Elliott, E. M.: Novel Method for Nitrogen Isotopic Analysis of Soil-Emitted Nitric Oxide, *Environ. Sci. Technol.*, 51, 6268–6278, <https://doi.org/10.1021/acs.est.7b00592>, 2017.

Zeldovich, Y. B.: The Oxidation of Nitrogen in Combustion and Explosions, *Acta Physicochim. Acad. Sci. USSR*, 21, 577–628, 1946.

890 Zong, Z., Wang, X., Tian, C., Chen, Y., Fang, Y., Zhang, F., Li, C., Sun, J., Li, J., and Zhang, G.: First Assessment of NO_x Sources at a Regional Background Site in North China Using Isotopic Analysis Linked with Modeling, *Environ. Sci. Technol.*, 51, 5923–5931, <https://doi.org/10.1021/acs.est.6b06316>, 2017.